Title: Spatiotemporal patterns of sleep spindle activity in human anterior thalamus and cortex

Authors:
Bernhard, Hannah [a,b]
Schaper, Frederic L. W. V. J. [c,e,h]
Janssen, Marcus L. F. [e,g]
Gommer, Erik D. [d,e,g]
Jansma, Bernadette M. [a,f]
Van Kranen-Mastenbroek, Vivianne [d,e,g]
Rouhl, Rob P. W. [c,d,e]
Weerd, Peter de [a,f]
Reithler, Joel * [a,f]
Roberts, Mark J. * [a,f]
DBS study group **

Affiliations:
a Department of Cognitive Neuroscience, Faculty of Psychology and Neuroscience, Maastricht University, Maastricht, The Netherlands
b Centre for Integrative Neuroscience, Maastricht University, Maastricht, The Netherlands
c Department of Neurology, Maastricht University Medical Center, Maastricht, the Netherlands
d Academic Center for Epileptology Kempenhaeghe/MUMC+ Maastricht and Heeze, the Netherlands
e School for Mental Health and Neuroscience, Maastricht University, Maastricht, the Netherlands
f Maastricht Brain Imaging Center (M-BIC), Maastricht University, Maastricht, the Netherlands
g Department of Clinical Neurophysiology, Maastricht University Medical Center, Maastricht, the Netherlands
h Center for Brain Circuit Therapeutics, Department of Neurology, Brigham and Women's hospital, Harvard Medical School, Boston, United States.

* shared senior co-authorship

** DBS study group: Wagner, Louis G.; Colon, Albert J.; Hilkman, Danny M.W.; Vlooswijk, Marielle C. G.; Nelissen, Jeske; Ackermans, Linda; Temel, Yasin

Correspondence: Hannah Bernhard (hannah.bernhard@maastrichtuniversity.nl); Department of Cognitive Neuroscience, P.O. Box 616, 6200 MD Maastricht, The Netherlands

Abstract

Sleep spindles (8 - 16 Hz) are transient electrophysiological events during non-rapid eye movement sleep. While sleep spindles are routinely observed in the cortex using scalp electroencephalography (EEG), recordings of their thalamic counterparts have not been widely studied in humans. Based on a few existing studies, it has been hypothesized that spindles occur as largely local phenomena. We investigated intra-thalamic and thalamocortical spindle co-occurrence, which may underlie thalamocortical communication. We obtained scalp EEG and thalamic recordings from 7 patients that received bilateral deep brain stimulation (DBS) electrodes to the anterior thalamus for the treatment of drug resistant focal epilepsy. Spindles were categorized into subtypes based on their main frequency (i.e., slow (10±2 Hz) or fast (14±2 Hz)) and their level of thalamic involvement (spanning one channel, or spreading uni- or bilaterally within the thalamus). For the first time, we contrasted observed spindle patterns with permuted data to estimate random spindle co-occurrence. We found that multichannel spindle patterns were systematically coordinated at the thalamic and thalamocortical level. Importantly, distinct topographical patterns of thalamocortical spindle overlap were associated with slow and fast subtypes of spindles. These observations provide further evidence for coordinated spindle activity in thalamocortical networks.

Highlights:

- Sleep spindles were measured in human anterior thalamus and on the scalp
- Both fast and slow spindles occurred in the anterior thalamus
- > 25% of spindles spanned multiple channels in thalamus and cortex
- A novel statistical approach confirmed that spindle co-occurrences were not random
- Cortical spindle patterns depended on thalamic involvement and spindle frequency

Keywords: thalamus, sleep spindle, thalamocortical coupling, human, intracranial EEG

Introduction

Sleep spindles are transient (0.3 – 2 s) electrophysiological patterns (8 – 16 Hz) and a characteristic of non-rapid eye movement (NREM) sleep in humans and other mammals (Fernandez & Lüthi, 2020). Recent research suggests that spindles may be involved in coordinating information transfer in hippocampal and neocortical networks to support memory consolidation and learning (Andrillon & Kouider, 2020; Klinzing et al., 2019; Latchoumane et al., 2017; Ngo et al., 2020; Staresina et al., 2015). Spindles across the brain can occur in a number of ways. They could be locally restricted to specific (cortical) sites or they could spread from thalamus to cortex in a set manner. Both options would preclude spindles from flexibly coordinating information transfer. Alternatively, spindles might follow function-specific spatiotemporal patterns. To the best of our knowledge, the extent to which spindles systematically co-occur within thalamic and across thalamocortical networks is unknown. Here, we investigated in humans whether sleep spindle activity in anterior thalamus and cortex follows coordinated spatiotemporal patterns.

To date, only few studies on human thalamic spindles exist. The reasons for this are twofold. Most human spindle research has relied on scalp electroencephalography (EEG), whose limited spatial resolution does not permit inferences about thalamic spindles. Thalamic signals can only be recorded using invasive procedures, but invasive thalamic recordings are generally performed during awake brain surgery or under anesthesia (Schaper et al., 2019). Deep brain recordings acquired via externalized deep brain stimulation (DBS) leads (Schreiner, Kaufmann, et al., 2021; Szalárdy et al., 2021), provide a safe (Feldmann et al., 2021) opportunity to study thalamic spindles in clinical populations of patients with epilepsy. Several studies have performed recordings from the posterior thalamus and cortex. For example, Mak-McCully et al. showed that thalamic spindles can precede spindles in neocortex (Mak-McCully et al., 2017). Bastuji et al. reported a tendency of localized thalamic spindles to also have more localized cortical counterpart, while diffuse thalamic spindles were correspondingly more diffusely represented in the cortex (Bastuji et al., 2020). Based on these data, the authors have inferred coordinated spindle activity across networks. However, their analysis did not account for random temporal overlap of spindle activity. In addition, these studies did not differentiate between so called slow (8 – 12 Hz) and fast (12 – 16 Hz) spindles. This differentiation seems relevant, because different types of spindles might have

95 different functions. Fast spindles have been linked to memory processes (Ngo et al., 2013). The
96 functional role as well as the physiology of slow spindles is understudied, as the majority of studies
97 filtered in the spindle frequency range of 11 to 16 Hz (Bastuji et al., 2020; Mak-McCully et al.,
98 2017). Furthermore, due to clinical constraints, these studies focused on the unilateral posterior
99 thalamus. Consequently, the spindle behavior within the anterior thalamus and between anterior
100 thalamus and cortex remains unknown. A characterization of spindles in the anterior thalamus is
101 pertinent, because of its relation to memory function in animals (Aggleton et al., 2010; Frost et al.,
102 2021) and humans (Sweeney-Reed et al., 2014, 2017, 2021).

103 Here, we addressed these issues and took a statistical approach to measure patterns of slow and
104 fast spindle (co-)occurrence in the anterior thalamus and cortex by controlling for random spindle
105 co-occurrence using permutation testing. This approach allowed us to compare temporal spindle
106 coupling observed in the data with distributions of random spindle co-occurrence, thereby
107 informing whether spindles in thalamocortical loops occur in systematically coordinated patterns.
108 We recorded data in 7 individuals with epilepsy who underwent implantation of DBS quadripolar
109 electrodes targeting the anterior nucleus of the thalamus (ANT). The setup of bilateral thalamic
110 depth electrodes allowed us to assess co-occurrences of thalamic spindles within and across
111 hemispheres. Simultaneous 19-channel scalp EEG recordings made it possible to study
112 thalamocortical spindle co-occurrence globally across the cortex. We categorized spindles based
113 on their main frequency as slow (10±2 Hz) or fast (14±2 Hz) spindles, as well as their level of
114 thalamic involvement (spindles restricted to one channel, or spanning more than one channel
115 unilaterally or bilaterally). We found that both slow and fast thalamic and thalamocortical spindles
116 were more likely to co-occur across channels than expected by chance. Additionally, distinct
117 topographical patterns of spindle overlap were associated with the different spindle subtypes.
118 These observations provide support that slow and fast spindle activity are systematically
119 coordinated in thalamocortical circuits.

120

Materials & Methods

Study design

The participants included in this study were admitted to Maastricht University Medical Centre for the implantation of DBS as treatment for drug-resistant focal epilepsy. In- and exclusion criteria followed the FDA and CE mark of the SANTE trial and are described elsewhere (Fisher et al., 2010; Salanova et al., 2015; Schaper et al., 2020). Patients were monitored with EEG and intracranial registration of their DBS electrodes for 22 hours after DBS implantation, including one night of sleep. The study procedure (DBSSEPI study (Dutch Trial Register NL4440 (NTR4562))) was approved by the medical ethical committee of Maastricht University Medical Centre, the Netherlands (ID: METC 14-4-126), and was conducted in accordance with the declaration of Helsinki.

Participants

Seven individuals with drug-resistant focal epilepsy were included in this study (2 female; mean age 35 years; range 18 – 59 years). Six other individuals, who were part of the DBSSEPI study (Schaper et al., 2019, 2020) were excluded due to missing scalp electrodes and/or seizures during the night of recording.

P	Sex	Age	Treatment (medication, dosage)	MRI abnormalities	EEG electrodes
1	m	26	levetiracetam 2d1000mg, oxcarbazepine 2d450mg, lacosamide 1d50mg, clobazam 3d5mg	Normal	19 channel
2	m	23	phenytoin 2d150mg, lamotrigine 2d250mg, perampanel 1d10mg	Normal	19 channel
3	m	59	carbamazepine 200mg-400mg, clobazam 1d5mg, lacosamide 2d200mg	generalized atrophy	19 channel
4	f	19	carbamazepine 2d200mg, lamotrigine 250mg-200mg, perampanel 1d2mg, topiramate 2d75m	Normal	19 channel
5	m	51	lacosamide 2d150m	Normal	22 channel (incl. EOG)
6	f	49	phenytoin 125mg-112,5mg, carbamazepine 2d600mg	frontobasal scars	22 channel (incl. EOG)
7	m	18	brivaracetam 2d100mg, carbamazepine 2d200mg, clobazam 2d10mg, lamotrigine 2d200mg	Normal	22 channel (incl. EOG)

Table 1. Individual clinical and MRI data and EEG setup.

DBS surgery

142 As part of standard clinical practice, all participants had a pre-operative 3-T MRI (Philips,
143 Eindhoven, The Netherlands) or 1.5-T MRI (Philips, Eindhoven, The Netherlands) in case of an
144 implanted vagal nerve stimulator for stereotactic planning of the electrode trajectory. The
145 sequences used were a 3D T1 with gadolinium, axial T2 and a T1 inversion recovery.
146 DBS electrode implantation was performed by directly targeting the ANT on pre-operative MRI.
147 The most distal contacts were placed at the termination point of the mammillothalamic tract
148 (MTT) in the ANT, also called the ANT-MTT junction (Lehtimäki et al., 2019). DBS surgery was
149 performed under general anesthesia with remifentanil and propofol using a Leksell stereotactic
150 frame, under guidance of intraoperative microelectrode recording. Details of the DBS surgery and
151 lead placement are described elsewhere (Schaper et al., 2019, 2020).
152
153 *DBS lead localization*
154 DBS leads were localized in a common space (Montreal Neurological Institute (MNI) 1522009b
155 template (Fonov et al., 2011)) using Lead-DBS software (https://www.lead-dbs.org) with default
156 settings (Horn et al., 2019), in line with previous studies (Horn et al., 2017). In short, pre-operative
157 T1 / T2 MRI sequences and post-operative MRI / CT images (suppl. table 1) were linearly co-
158 registered using SPM (Friston et al., 1994), version 12. Co-registration was further refined using
159 the *brainshift correction* option (Schönecker et al., 2009) and images were normalized to MNI
160 space using the Advanced Normalization Tool (http://stnava.github.io/ANTs/; Avants et al., 2008).
161 DBS electrode trajectories and contacts were automatically pre-localized and manually refined
162 using Lead-DBS. DBS lead trajectories were visualized in MNI space in relation to a thalamic mask,
163 derived from the Thomas atlas (Su et al., 2019) and can be seen in figure 1.
164

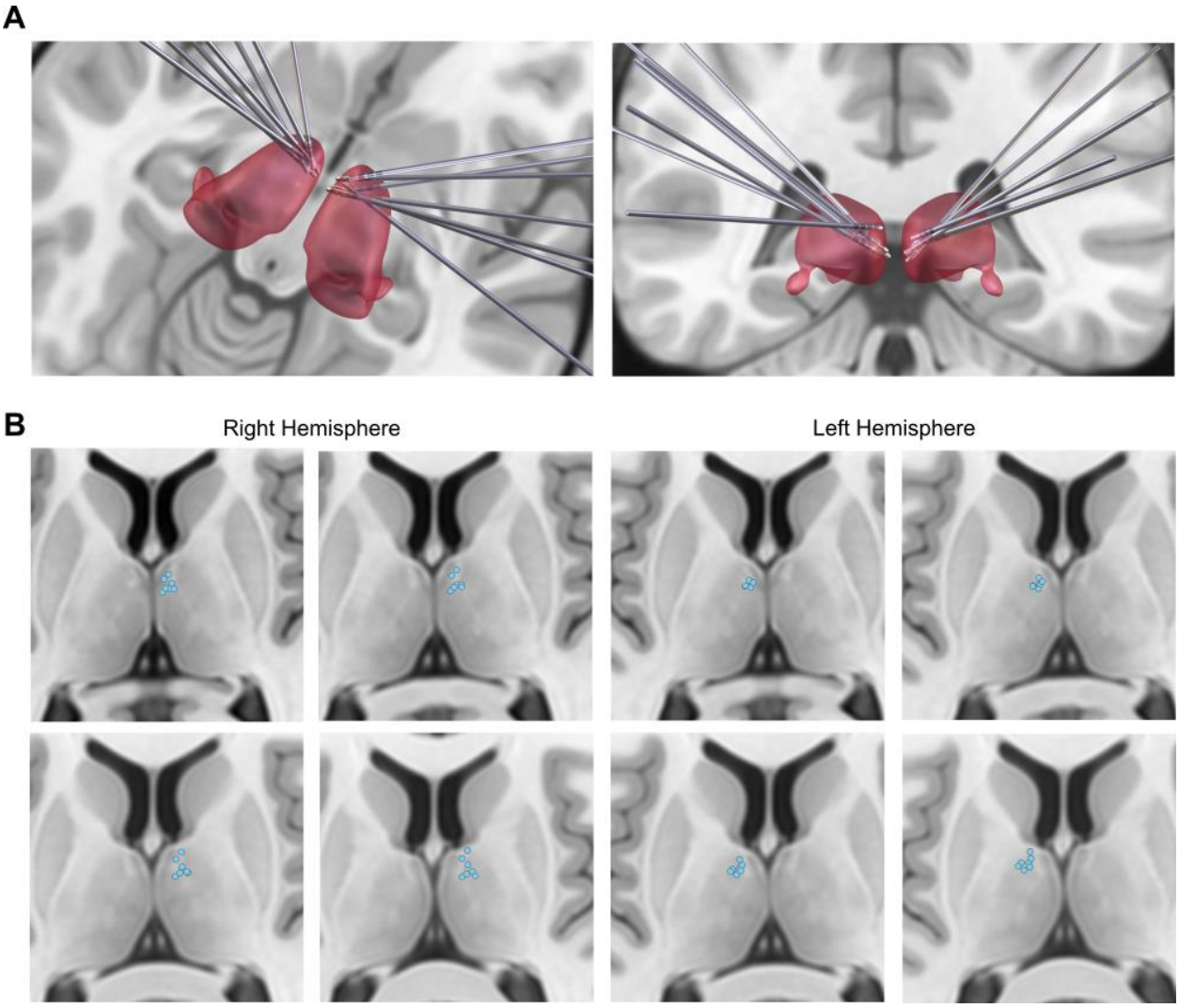

Figure 1. DBS lead locations and anterior thalamic recording sites in a common atlas space. **A)** Bilateral trajectories of implanted DBS leads for all participants (n=7) in transversal (left) and coronal (right) view. Note that each lead contained four electrode contacts. **B)** Contact positions (blue dots) of all participants projected onto a thalamic mask derived from the Thomas atlas (Su et al., 2019). MNI coordinates of each contact can be found in supplementary table 1.

Data acquisition of electrophysiological recordings

Thalamic local field potentials (LFPs) were acquired using quadripolar externalized DBS leads (model 3389, Medtronic, Dublin, Ireland). Scalp EEG was measured using a 19-channel setup, with Ag/AgCl cup electrodes placed according to the standard 10-20 system. Data were recorded in Brain RT version 3.3 at a sampling rate of 2048 Hz, using Braintronics BrainBox-1166-64.

178 *Sleep scoring*

179 Sleep scoring was performed in Brain RT version 3.3. For three out of seven participants, eye
180 movement activity was measured with electro-oculogram (EOG) electrodes placed on the outer
181 corners of the eyes, recording horizontal (HEOG) and vertical (VEOG) eye movements,
182 respectively. For sleep scoring, a bipolar montage was applied to HEOG and VEOG channels,
183 respectively. Four patients did not have EOG recordings. In this case, the frontal scalp EEG channels
184 (Fp1 and Fp2, as well as F7 and F8, respectively) were re-referenced to bipolar derivations to show
185 maximum eye movement activity for the polysomnographic scoring (i.e., Fp1 to F7, and Fp2 to F8),
186 enabling the identification of wake and phasic REM periods. Channels F3, C3, O1, were re-
187 referenced to the right mastoid, channels C4 and O2 to the left mastoid. Using a notch-filter at 50
188 Hz and a window size of 30s, a sleep scoring expert (H.B.) manually scored the data into sleep
189 stages according to the American Academy of Sleep Medicine (AASM) criteria (Berry et al., 2015).

190

191 *Data Preprocessing*

192 The Fieldtrip toolbox (Oostenveld, Fries, Maris, & Schoffelen, 2011; http://fieldtriptoolbox.org),
193 Sleeptrip toolbox (), MATLAB R2018a and 2021b (Mathworks Inc., Sherbom, MA) were used for
194 data analysis. Hypnograms and continuous data were exported from Brain RT to Matlab. A high
195 pass filter at 0.4 Hz (Butterworth, two-pass filter, 5th order) was applied to the continuous data,
196 before down-sampling to 512 Hz. Electrodes were checked manually and, in case of continuous
197 high noise levels, excluded. This was only the case for one electrode (A2) in one participant.

198 Scalp EEG activity was then re-referenced to the average of the mastoid electrodes (A1, A2), or to
199 the average of all scalp electrodes for the patient missing A2. For the thalamic electrodes, bipolar
200 derivations were computed between neighboring electrodes, resulting in 6 thalamic channels per
201 participant (3 per hemisphere). We chose bipolar derivations to obtain a more localized signal.
202 Where a certain thalamic nucleus is named in the supplementary material of this paper, one or
203 both of the electrodes in the bipolar derivation were localized within this nucleus. However, given
204 the length (1.5mm), diameter (1.27 mm) and spacing (0.55 mm) of electrode contacts, bipolar
205 derivations may not be located in one nucleus but span several.

Both thalamic LFP and scalp EEG data were subjected to a low pass filter at 100Hz (Butterworth, two-pass, 5th order), and a line noise filter at 50 Hz to reduce electrical noise. Subsequently, the continuous data were transformed into 30 s epochs and linked with the sleep hypnogram. Epochs with manually identified artifacts (e.g., visibly noisy signal) or arousals were excluded, as well as any epochs not pertaining to NREM sleep (N2 and N3, respectively).

Spindle detection

Automatized spindle detection was performed in Sleeptrip, based on a pipeline used in previous literature (Weber et al., 2020). Spindles were detected in NREM sleep. To summarize, data from NREM segments were subjected to a FIR filter with a peak-frequency of 10 ± 2 Hz for slow and 14 ± 2 Hz for fast spindles, respectively. Next, the absolute value of the Hilbert transform of the filtered signal was taken to detect the spindles. Segments in which the envelope surpassed the threshold of the mean ±1.5 SD were marked as putative spindles. If the threshold crossings fell into the duration limits of 0.3 to 2 s, and a second threshold of 2.25 SD was passed at least once, these segments were considered as spindles. Spindles were not merged if they closely followed each other. Spindle detection was implemented separately for each channel and participant.

Spindle detection control analysis

To verify that detected time windows included true spindles and not false positives, e.g. due to broadband frequency changes, we implemented a control analysis based on Ngo et al. (2020). This control analysis was done separately for slow and fast spindles. For each channel, time-frequency representations (TFRs) of each spindle were created using wavelets (5 cycles; 5 to 15 Hz for slow spindles; 9 to 19 Hz for fast spindles; in 0.5 Hz steps, time window of ± 0.75 s in 2 ms steps). Per event, frequencies were averaged between - 0.5 to + 0.5 s. Then, the *findpeaks* function was used on the resulting spectrogram. A putative spindle was considered a true spindle when the peak surpassed 0.2 prominence, and if the peak was between 8 to 12 Hz (for slow spindles) or 12 to 16 Hz (for fast spindles). All false positives were excluded from further analyses. For the number of detected spindle events and those that passed the control analysis, see table 2.

235 *Spindle characteristics*

236 To quantify spindle parameters in the anterior thalamus, we computed several descriptive
237 measures per channel and per participant for slow and fast spindles separately, namely: Spindle
238 duration (difference of spindle offset and onset); spindle density (number of spindles per minute)
239 and spindle amplitude (maximum peak to trough potential difference). Putative differences of
240 spindle characteristics between fast and slow spindles were compared using paired t-tests per
241 channel, setting the two-tailed significance level at $\alpha = 0.05$. In a separate step, we examined
242 whether channels in certain nuclei differed in spindle characteristics (supplementary material and
243 supplementary figure 2), but caution against their overinterpretation due to several factors: Our
244 definition of the exact nucleus can only be viewed as an approximation, the number of electrode
245 contacts differ between thalamic nuclei, and the age range of the sample may lead to variability
246 within a given nucleus.

247 To visualize the presence of slow and fast spindles in the thalamic LFP, we selected time-windows
248 of ±1 s around the midpoint of algorithmically detected slow and fast spindles. Next, the TFR of
249 each spindle was created using wavelets (5 cycles; 6 to 18 Hz, time window of ± 0.75 s in 1 ms
250 steps), and TFRs were averaged separately for time-windows marked as slow or fast by the
251 algorithm. To visualize the spatial layout of spindles in the scalp EEG, density values per scalp
252 electrode were averaged across participants, separately for the algorithmically detected slow and
253 fast spindles.

254

255 *Thalamic and thalamocortical spindle co-occurrence*

256 To evaluate whether spindles occurred in isolation or co-occurred across channels, we created
257 continuous spindle time-courses across all channels. That is, a channel x time point matrix
258 spanning the total duration of artifact-free NREM sleep was marked with absence or presence of
259 spindles (0 or 1, respectively). The continuous spindle time-courses of a participant's channels
260 were divided into separate spindle events as follows: First, each time point was summed across
261 channels. The resulting vector contained information on how many channels showed spindle
262 activity at a given time point. Time points with 0 values meant no spindle activity occurring in any

263 of the channels, and served to define boundaries between individual spindles. Time points with
264 values > 0 were categorised as a (co-)occurring spindle.
265 We refer to the different combinations of thalamic and thalamocortical channels participating in
266 a spindle event as spindle scenarios. Figure 2B schematizes these spindle scenarios at the thalamic
267 (T spindles, 2B.I), the thalamocortical (TC spindles, 2B.II) and the cortical (T_0C spindles, 2B.II) level.
268 At the thalamic level, spindles were further categorized into clusters spanning 1 to 6 channels (T_1
269 to T_6 spindles, according to the number of thalamic channels involved in each spindle event).
270 Spindle events occurring in >1 thalamic channel were further categorized as unilateral or bilateral,
271 depending on whether they occurred in one hemisphere (unilateral; fig. 2B.I & II, second column)
272 or in both (bilateral; fig. 2B.I & II third column). Because we recorded from 3 channels in each
273 thalamic hemisphere, spindle clusters T_4 or greater were bilateral by definition, while T_2 and T_3
274 could be either unilateral or bilateral clusters.
275 Given the difference in spindle numbers per scenario and participant, rates of each scenario are
276 reported as the percentages rather than as raw counts. The analysis was carried out separately for
277 thalamic and thalamocortical spindles. For thalamic spindles, we did not consider scalp EEG
278 activity, and report the spindle events per thalamic channel as a percentage of all thalamic spindle
279 events. For thalamocortical spindles, the information about spindle occurrence of all scalp EEG
280 channels were collapsed into one cortical channel (Fig. 2B.II). That is, whenever a spindle occurred
281 in one scalp EEG electrode, this was marked in the common scalp channel. Thalamocortical spindle
282 events are reported as a percentage of all spindle events occurring across thalamus and cortex.
283 We refer to thalamocortical spindles as T_xC, where X correspond to the number of thalamus
284 channels involved. In addition, we recorded how many scalp EEG spindle events did not have a
285 thalamic counterpart as a percentage of the total number of detected spindles across all channels
286 in a participant (T_0C; Fig. 2B.II, fourth column). All analyses were computed separately for slow and
287 fast spindles.
288

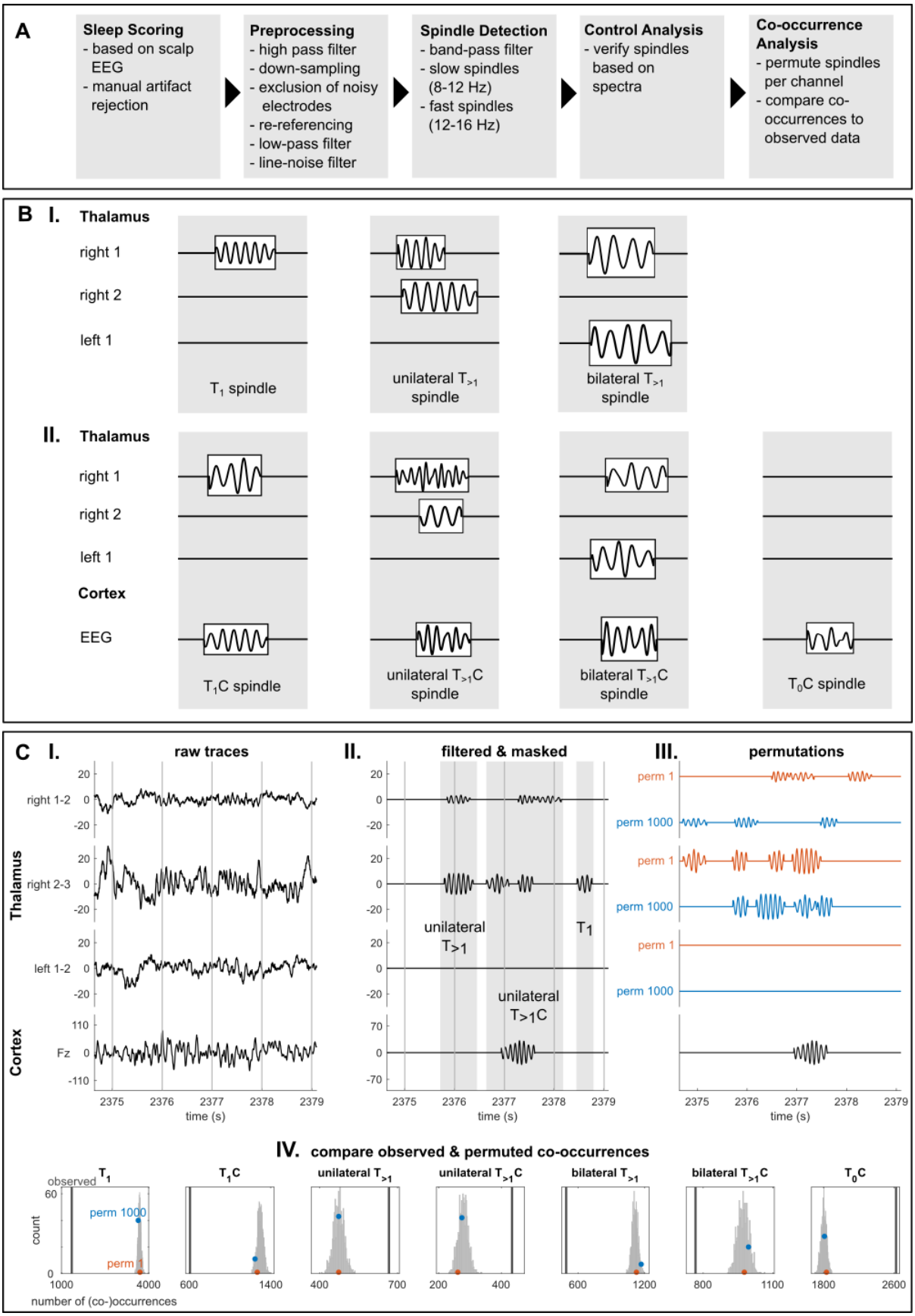
A
Sleep Scoring
- based on scalp EEG
- manual artifact rejection
Preprocessing
- high pass filter
- down-sampling
- exclusion of noisy electrodes
- re-referencing
- low-pass filter
- line-noise filter
Spindle Detection
- band-pass filter
- slow spindles (8-12 Hz)
- fast spindles (12-16 Hz)
Control Analysis
- verify spindles based on spectra
Co-occurrence Analysis
- permute spindles per channel
- compare co-occurrences to observed data
B I. Thalamus
right 1
right 2
left 1
T1 spindle
unilateral T>1 spindle
bilateral T>1 spindle
II. Thalamus
right 1
right 2
left 1
Cortex
EEG
T1C spindle
unilateral T>1C spindle
bilateral T>1C spindle
T0C spindle
C I. raw traces
II. filtered & masked
III. permutations
Thalamus
right 1-2
right 2-3
left 1-2
Cortex
Fz
unilateral T>1
T1
unilateral T>1C
perm 1
perm 1000
time (s)
IV. compare observed & permuted co-occurrences
observed
perm 1000
perm 1
count
number of (co-)occurrences
T1
T1C
unilateral T>1
unilateral T>1C
bilateral T>1
bilateral T>1C
T0C

289

290 **Figure 2.** Overview of (pre-)processing steps to measure spindle (co-)occurrence in thalamic and scalp signals. **A)**
291 Sequence of pre-processing steps and spindle detection. **B)** Schematized overview of spindle scenarios, i.e.,
292 possible channel combinations involved in a thalamic (**B.I**) or thalamocortical (**B.II**) spindle event. Three thalamic
293 (2 right, 1 left) channels and the cortex time-course (all scalp EEG activity collapsed into one channel) are
294 schematized. Subscripts describe the number of thalamic channels participating in a given spindle, so that a T_1
295 spindle describes a spindle occurring in one thalamic channel. For more data examples for the spindle scenarios,
296 see supplementary figure 1. **C)** Analysis steps are visualized on a data segment from three thalamic (2 right, 1
297 left) channels and one cortical channel (Fz) of one participant. Shown are an example raw trace (**C.I**) and filtered
298 signal (**C.II**), in which only the detected spindles are shown and other data are masked. The grayscale columns
299 mark (co-)occurring spindle activity and categorization of the shown spindles according to the spindle scenarios
300 detailed in B). **C.III** depicts exemplar permutations of this data segment. Note that NREM time points were re-
301 shuffled in each thalamic channel keeping the number and duration of spindles constant. The observed and
302 permuted (co-)occurrences were then compared, as visualized in **C.IV**. Per spindle scenario, the number of co-
303 occurrences were counted in the observed (black line) and permuted data (permutation 1 and 1000 are
304 indicated in the histogram with the y-values at the lowest and highest bin-counts, respectively). To evaluate the
305 likelihood of the observed value stemming from the permuted distribution, we assessed the proportion of
306 permuted values that were more extreme than the observed value. In the analysis of thalamic and
307 thalamocortical spindle clusters, we report the difference between the observed value and the mean of the
308 permuted distribution. Note that the observed value and permuted distributions are shown as untransformed
309 data for visualization purposes, but that we report percentages to enable comparison across subjects.
310

311 *Thalamocortical spindle co-occurrence maps*

312 To evaluate putative topographical differences in thalamocortical spindle co-occurrence for the
313 thalamic spindle scenarios (T_1C, unilateral or bilateral $T_{>1}C$), we focused on the continuous spindle
314 time-courses across individual scalp EEG channels. To measure the co-occurrence of thalamic
315 spindles with cortical spindles, we considered each thalamus channel as seed and each cortical
316 channel as target channels. Only time points were included during which the seed and at least one
317 cortical channel showed spindle activity. The spindle activity overlap was then calculated as the
318 proportion of time points during which the target channel showed spindle activity at the same
319 time as the seed channel out of the total number of T_1C, unilateral or bilateral $T_{>1}C$ spindle time
320 points of a seed channel. That is, in order to have 100% overlap with T_1C spindles, the target
321 channel would need to show spindle activity at all the time points that the seed channel was

322 engaged in a spindle with no other thalamic channel showing simultaneous spindle activity.
323 Consequently, a 50% overlap with T_1C spindles would signify that only half of the target's spindle
324 activity temporally coincided with the seed's spindle activity, when this particular thalamic seed
325 channel showed a spindle that was not shared by any other thalamic channels. This analysis was
326 carried out for each of the six thalamic channels, and separately for slow and fast spindles.
327
328 *Paired time-lag analysis of thalamocortical overlap*
329 Thalamocortical overlap maps were calculated at a 0 time-lag, and thereby might not capture
330 time-delayed relationships between seed and target channels. To evaluate whether there were
331 any consistent non-zero time-lag relationships between seed and target channels across
332 participants, histograms for the time lag between the onset of seed and target spindles were
333 computed, sorted into bins of 0.05 s between ±0.75 s and averaged across seed, target channels
334 and participants. The resulting histograms contain the average distribution of lags between
335 thalamus and cortex, for which we tested the difference from 0 by means of a one-sample t-test.
336
337 *Within-participant statistical analyses*
338 Spindle co-occurrence across channels may happen by chance according to the number and
339 duration of spindles in a given channel pair. To test whether and to what extent observations of
340 thalamic or thalamocortical spindle co-occurrence were due to chance, we tested within-
341 participant statistical significance by permuting the data 1000 times. Figure 2C.III and IV visualizes
342 this procedure. The time points of artifact-free NREM sleep of each thalamic channel were
343 shuffled, keeping number and duration of spindles constant. Spindle co-occurrences in the
344 permuted data were quantified as in the observed data, by using 0-columns in the channel x time
345 matrix as bounds between spindle events (as shown in 2C.II). When permuting the data, $T_{>1}$
346 spindles may be broken up into many T_1 spindles, thus permuted data could contain a higher total
347 number of spindle events than the original data. In order to keep permuted and non-permuted
348 data comparable, we assessed the counts of spindle clusters as percentages of the sum of spindle
349 events in a given participant and permutation. For the analysis of slow and of fast thalamic spindle
350 clusters, we report the observed spindle events as the percentage of all respective spindle events

351 across all thalamic channels. We repeated this analysis for slow and fast thalamocortical spindles
352 separately, where we report the observed spindle events as the percentage of all respective
353 spindle events across thalamic and cortical channels.
354 For statistical testing, the permuted and non-permuted data were z-scored based on the mean
355 and standard deviation of the permuted data. The z-scored percentage of spindles in the non-
356 permuted data were tested two-sided against the z-scored permuted distribution of percentage
357 of spindles, with the p-value calculated as the proportion of permuted values that were more
358 extreme than the observed value. For a visualization of the comparison between observed and
359 permuted data, consider figure 2C.IV, which depicts exemplar permuted distributions and
360 observed values for each of the thalamic and thalamocortical spindle scenarios for one participant.
361 Lastly, the difference percentage of observed and mean permuted spindle clusters was computed.
362 Positive values thus indicate cases in which specific spindle scenarios occurred more frequently in
363 the observed than permuted data (e.g. 2C.IV, unilateral $T_{>1}C$ spindles), whereas negative values
364 reflect spindle scenarios that occurred less frequently in the observed than permuted data (e.g.,
365 2C.IV, T_1 spindles). Consequently, scenarios that are more likely in the observed than permuted
366 data suggest systematic temporal co-occurrence of spindle activity.
367 For mapping thalamocortical spindles, temporal spindle overlap was quantified based on the
368 continuous spindle time-courses. Hence, the permuted data were not separated into spindle
369 events, but quantified as the overlap of spindle time points of the target electrode with the seed
370 electrode. The overlap thus describes the percentage of time a channel pair engages in spindle
371 activity simultaneously. Only channels with p-value < 0.025 (indicating an observed value more
372 extreme on either side of the permuted distribution) were considered in further analyses.
373
374 *Group level statistical analyses*
375 Between-participant effects were tested by running repeated measures analysis of variance
376 (RMANOVA) on the difference in spindle percentage between observed and permuted values.
377 Where sphericity was violated, Greenhouse-Geisser corrected degrees of freedom are reported.
378 For significant main and interaction effects, post-hoc pairwise comparisons were computed and

adjusted for multiple comparisons using Bonferroni correction, and confidence intervals (Cis) at 95% are reported. The significance level was set at $\alpha = 0.05$.

For analysis of thalamic spindle clusters, a RMANOVA was computed with factors *cluster size* (1…6 channels involved) and *spindle type* (slow vs. fast). For testing thalamic uni- vs. bilateral involvement, the RMANOVA factors were *cluster size* (2 vs. 3 channels involved), *hemispheric involvement* (unilateral vs. bilateral) and *spindle type* (slow vs. fast). To assess the thalamocortical spindle behavior, the following RMANOVA factors were defined: *thalamic involvement* (T_1, unilateral or bilateral $T_{>1}$), *cortical involvement* (T vs. TC spindles) and *spindle type* (slow vs. fast). EEG spindle events that did not have a thalamic counterpart were compared between slow and fast spindles, using paired samples t-tests.

To investigate thalamocortical maps across participants, we computed the median difference of observed from permuted thalamocortical overlap across thalamic seed channels, hemispheres and participants, but separately per *spindle type* (slow vs. fast spindles), and *thalamic involvement* (T_1C, unilateral or bilateral $T_{>1}C$). We only included datapoints that were significantly different from permuted data at the within-participant level.

To qualitatively compare the topographies of different spindle types and thalamic classes, we computed the center of gravity (CoG) per category. CoG quantifies the mean location of thalamocortical overlap, as the average x- and y-position of all electrodes weighted by their values of thalamocortical overlap. The x- and y-position are both relative to the central EEG electrode (Cz) and indicate lateralization and placement on the anterior/posterior axis, respectively. Given that thalamocortical maps were averaged across hemispheres, positive, zero and negative lateralization values describe ipsilateral, midline and contralateral locations, respectively. Positive, zero and negative y-values describe anterior, central and posterior locations, respectively. To test the robustness of estimating the CoG based on the average maps, we used a bootstrapping approach, in which we resampled the population of statistically significantly overlapping scalp EEG channels (n = 42), with replacement 1000 times. For each iteration, a new CoG was computed per condition (spindle type and thalamic involvement). Additionally, the difference between slow and fast spindles for each thalamic class was calculated for x and y coordinates, respectively.

Statistical testing was carried out to evaluate whether the CoG was significantly lateralized and/or shifted along the anterior/posterior axis for each of the thalamic classes and spindle types. For this, we tested the difference of each of the 6 bootstrapped distributions from 0, both for the x- and y-coordinates, by calculating the proportion of cases < 0 in each distribution. Next, we evaluated whether the difference of lateralization and/or shift along the anterior/posterior axis differed between slow and fast spindles, by calculating the proportion of cases < 0 in the distribution of the difference.

Data availability

The data sets analyzed in the current study are not publicly available due to privacy concerns as outlined in the consent form.

Results

To investigate thalamocortical spindle co-occurrence we analyzed data recorded from 7 participants during one night of sleep. On average, participants slept for 8.15 ± 1.55 hours (489 ± 93 minutes), of which 5.98 ± 1.46 hours (359 ± 87.33 min) were spent in NREM sleep (stages N2 and N3; see table 2 for participant-specific details of minutes spent in each sleep stage). We algorithmically detected slow and fast spindles in a total of 42 bipolar thalamic channels (6 per participant) and 133 scalp EEG electrodes (19 per participant). Note that because electrode placement into the specific subnuclei varied inter-individually, we assessed spindles in the anterior thalamus as a whole rather than its subnuclei. Accordingly, we generally refer to the anterior thalamus as the broad region. In contrast, we refer to the specific subnucleus as the anterior nucleus of the thalamus or ANT.

Table 2 reports the number of putative spindle events detected in the thalamic LFP and scalp EEG per participant, and the number of spindle events after the spindle control analysis. Only spindle events that passed the control analysis were included in all further analyses.

Participant	1	2	3	4	5	6	7
Sleep stages							
wake	121.5	14.5	124	41	118	27.5	141.5
N1	118	25.5	164	35.5	38.5	54.5	221.5
N2	324.5	93.5	223.5	208	157	177.5	258
Artifact-free	315	79.5	181	200.5	141.5	155.5	248.5
N3	101.5	418.5	110	117.5	97.5	195.5	30.5
Artifact-free	101	376.5	91.5	115	90	183.5	30
REM	38.5	37	0	47.5	31	72.5	24.5
Spindle events							
Thalamus							
slow	23555	29316	18991	20339	17431	26645	18622
corrected	12656	8399	12588	12640	7587	18399	12243
fast	22779	28696	17148	18872	14220	20642	16697
corrected	12475	9937	2836	6130	2283	5271	5402
Cortex							
slow	81181	99071	63906	69564	46902	108052	64270
corrected	50359	17247	14969	27419	7908	83608	43461
fast	102576	103823	63155	76032	47722	79243	59343

corrected	72181	32085	19625	26515	9744	12521	21622

Table 2. Overview of participants' sleep architecture and detected spindle events before and after control analysis (corrected). Sleep staging data are reported in minutes, for spindle events the total number of events are reported (pooled across thalamic or scalp EEG electrodes, respectively).

Slow spindles occur more frequently in anterior thalamus than fast spindles

We first investigated whether slow and fast spindles were present in the anterior thalamus and scalp EEG. Both slow and fast spindles were present in all participants. Figure 3 A shows an example of a slow followed by a fast spindle in one participant (for another example, see supplementary figure 1 B). The average TFRs of all slow and fast spindles in the same channel are shown in figure 3B. Note that the TFRs were computed across the slow and fast spindle band. Consequently, if the distinction into slow and fast spindles were arbitrary, this should be seen by an overlap in the TFR. Figure 3C depicts the average slow and fast spindle distributions in the scalp EEG across all participants.

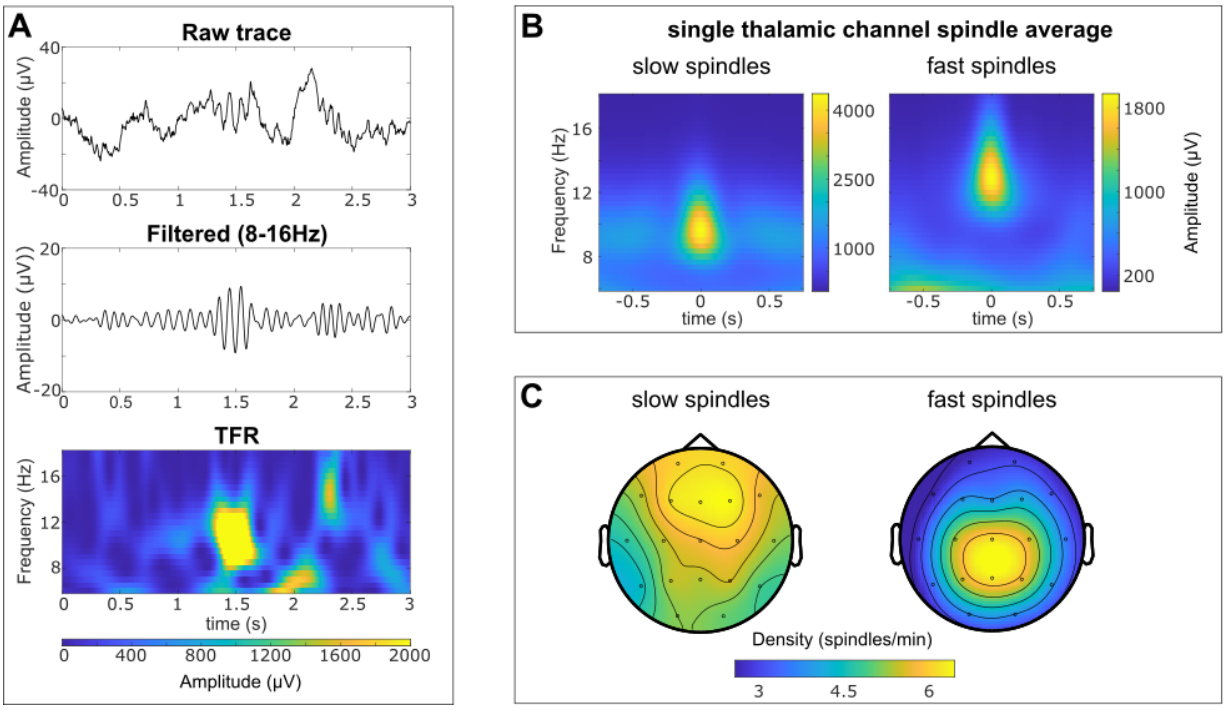

Figure 3. Slow and fast spindles in anterior thalamus and scalp EEG. **A)** Data of a slow (at 1.5 s) and fast (at 2.25 s) thalamic spindle, here represented in the raw trace (top panel), filtered trace (middle panel) and time-frequency representation (TFR; bottom panel). Data are shown for right thalamic channel 2-3 of participant 3.

B) Averaged TFRs centered on time windows containing slow (left) and fast (right) spindles in one thalamic channel. The represented channel is the same as in A. **C)** Density of slow (left) and fast (right) spindles in scalp EEG averaged across all subjects.

Next, we assessed whether anterior thalamic spindles differed in their density, duration or amplitude. Figure 4 shows the spindle density (A), duration (B) and amplitude (C) for slow and fast spindles. Both data pooled across thalamic channel per participant (top row) are shown, as well as the histograms of the differences (slow – fast spindles) at the channel level (bottom row). On average, spindle density (fig. 4A) was higher ($t(41) = 5.52$; $p < 0.001$) for slow (6.34 ± 3.22 spindles/min) than fast spindles (3.01 ± 1.46 spindles/min). Spindle duration (fig. 4B; $t(41) = 1.45$; $p = 0.15$) and spindle amplitude (fig. 4C; $t(41) = 1.97$; $p = 0.06$) did not differ between slow and fast spindles.

We evaluated the same descriptive spindle measures when categorizing the data according to their corresponding estimated thalamic nuclei (suppl. material and suppl. fig. 1) and did not find any differences between thalamic nuclei.

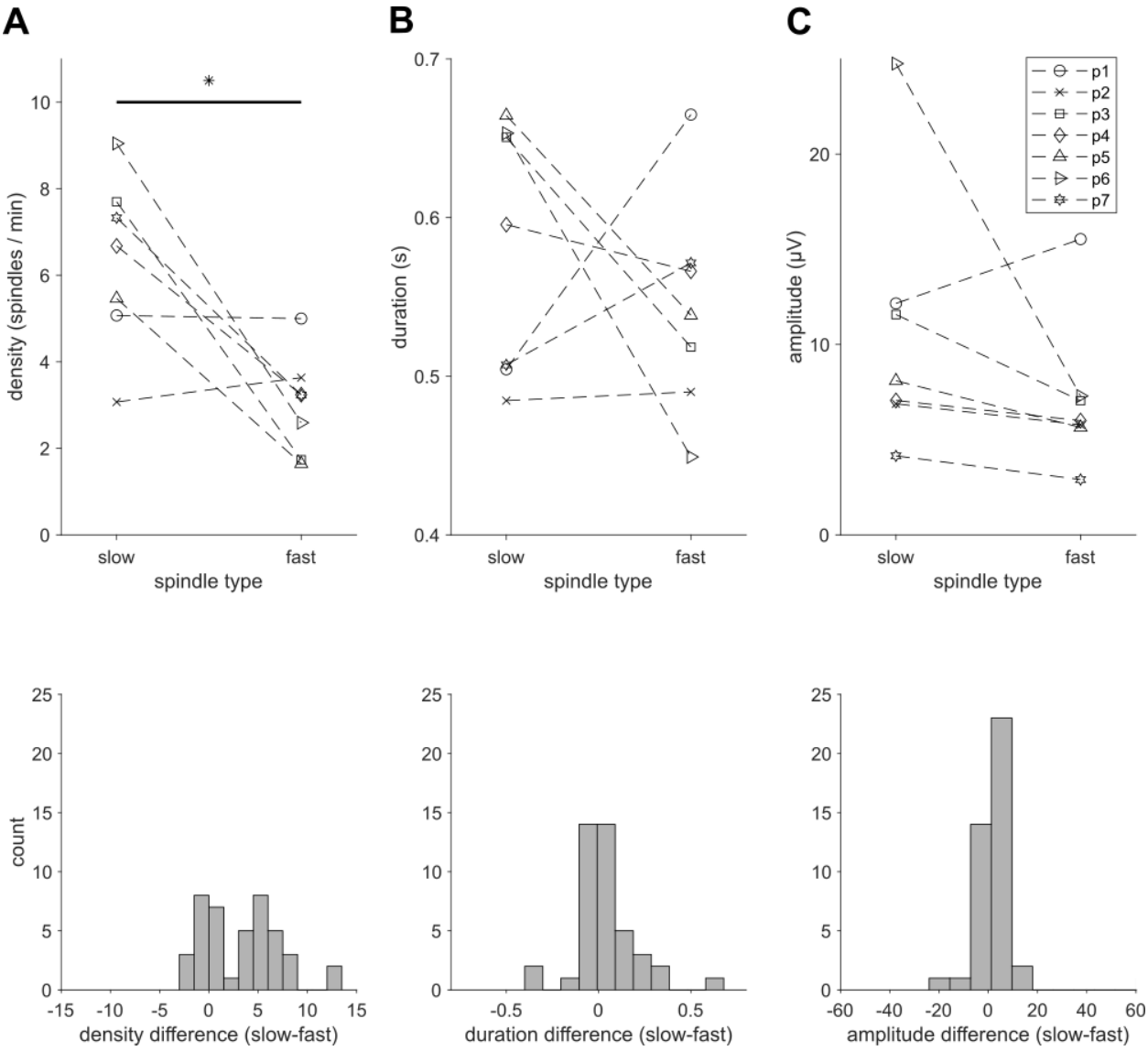

Figure 4. Spindle characteristics in anterior thalamus. Electrodes pooled per participant are shown (p1 to 7, legend) for slow and fast spindles (top row) and histograms of the differences (slow-fast) per electrode (bottom row). **A)** Average spindle density (number of spindles per minute) was on average higher for slow than for fast spindles; **B)** Spindle duration and **C)** spindle amplitude (peak to trough difference) did not differ between slow and fast spindles. Asterisk marks paired t-test difference significant at $p < 0.05$ (uncorrected).

Characterization of spindles in the anterior thalamus

In a next step, we investigated whether slow and fast spindles co-occurred across channels in the thalamus (without considering the cortical EEG channels). We refer to the number of thalamic channels involved in a spindle as a channel cluster. Figure 5A depicts the channel cluster size of

479 spindle events as a proportion of all thalamic spindles, separately for slow (upper panel) and fast
480 (lower panel) spindles. To control for random spindle co-occurrence, we next ran permutations of
481 the spindle time courses, with number and duration of spindles at each channel kept constant.
482 These permuted data allowed us to estimate how often spindles occurred in isolation or co-
483 occurred by chance. We compared these observed distributions of spindle clusters with the
484 permuted distributions. Figure 5B shows the population difference between observed and
485 permuted data for all 6 channel clusters for slow and fast spindles, respectively. Since the spindle
486 cluster sizes are expressed in percentages, the likelihoods of T_1 and $T_{>1}$ clusters are interdependent
487 and should be interpreted accordingly. T_1 spindles, which were the most dominant type in the
488 observed data (cf. fig. 5A), were less likely to occur in the observed compared to the permuted
489 data. In contrast, spindle co-occurrences ($T_{>1}$) occurred more often than expected by chance ($F_{1.29,}$
490 $_{7.71}$ = 119.41; $p < 0.001$ in RMANOVA; mean differences of observed – chance values between
491 spindle cluster of T_1 spindles vs. $T_{2...6}$ channels range from -26.65 to -35.13 %; $p \leq 0.001$). This
492 suggests that thalamic spindles co-occur more often than would be assumed based on permuted
493 distributions. Slow and fast spindles did not co-occur differently in the anterior thalamus ($F_{1,6}$ =
494 0.18; p = 0.69).
495 It is noteworthy that some spindle events spanned more than three channels, pointing to the
496 bilateral involvement of the thalamus in these spindle events (since our setup included three
497 channels in each thalamic hemisphere). We subdivided the observed T_2 and T_3 clusters to
498 investigate whether spindle clusters of two or three channels involved one or both hemispheres
499 of the thalamus. Figure 5C depicts the difference in proportion of unilateral and bilateral T_2 and T_3
500 spindles between observed and permuted data, for slow and fast spindles, respectively.
501 T2 and T3 spindles showed distinct unilateral and bilateral involvement ($F_{1,6}$ = 128.17; $p < 0.001$ in
502 RMANOVA). We observed that unilateral T_2 spindles occurred more often than by chance (15.58
503 %; 95 % CI, 11.99 to 19.18), while bilateral T_2 spindles occurred less often than by chance (-5.68
504 %; 95 % CI, -7.46 to -3.89). This can also be seen in figure 5C when looking at the T_2 data. This
505 difference between unilateral and bilateral spindles was absent for T_3 spindles: in this situation,
506 both unilateral (3.36 %; 95 % CI, 1.95 to 4.77) and bilateral spindles (4.81 %; 95 % CI, 3.32 to 6.31)
507 occurred equally more often than by chance (cf. fig. 5C, both unilateral and bilateral T_3 bars are

positive). We also observed a difference in the amount of slow and fast spindles spanning 2 or 3 channels in the thalamus ($F_{1,6}$ = 7.88; p = 0.03 in RMANOVA). There were more fast T_2 spindles (6.66 %; 95% CI, 4.21 to 9.12) than slow T_2 spindles (3.24 %; 95% CI, 0.14 to 6.34), but equally many slow (4.44 %; 95% CI, 3.70 to 5.18) and fast T_3 spindles (3.74 %; 95% CI, 2.56 to 4.93).

To conclude, these analyses indicated that compared to the permuted data, T_2 spindles tended to be unilateral, whereas T_3 spindles were equally likely unilateral or bilateral. Overall, it seems that thalamic spindle events did not only co-occur across channels, but were temporally coordinated within and across thalamic hemispheres.

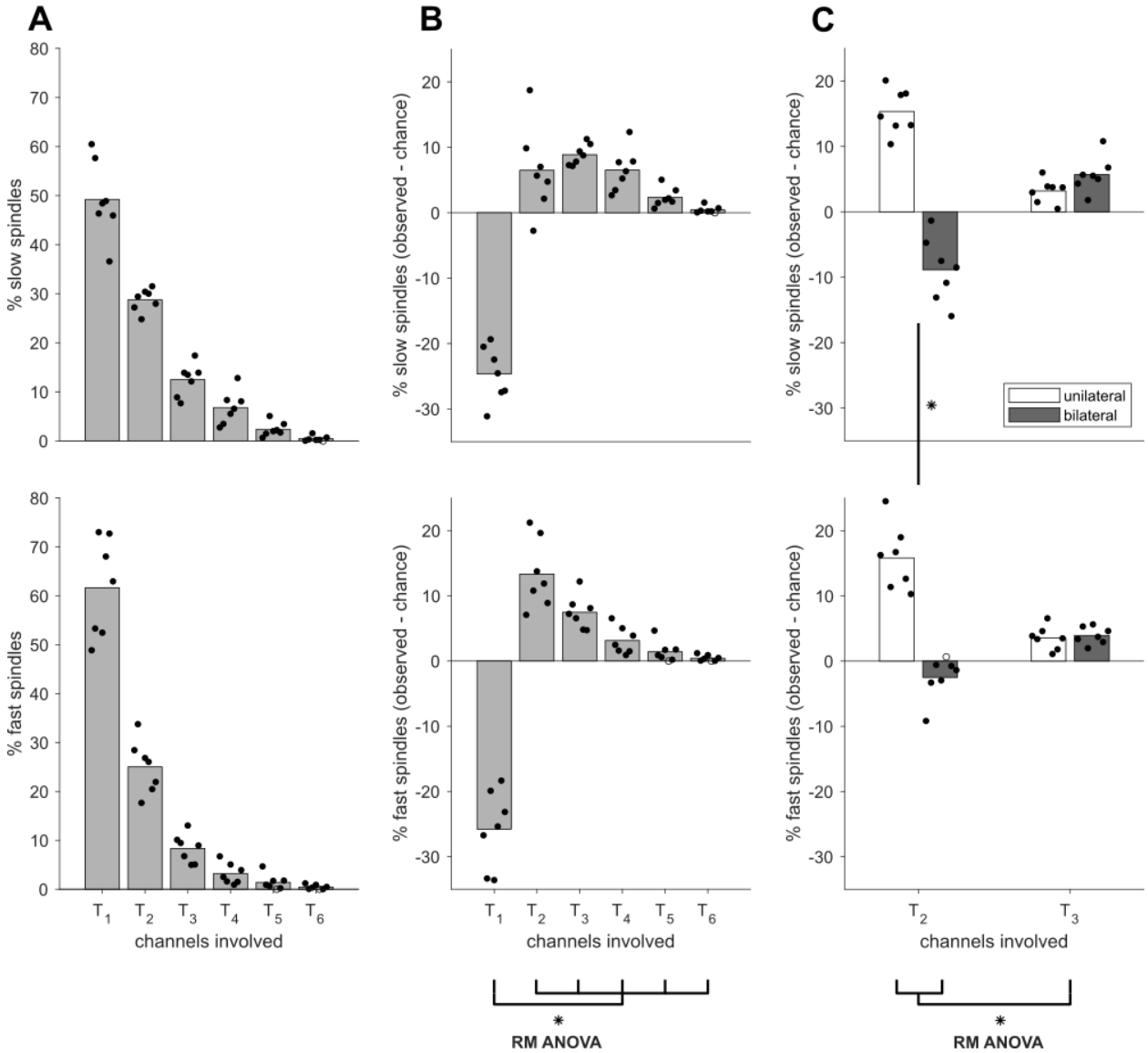

518 **Figure 5.** Observed thalamic spindles and the number of thalamic channels they spanned (channel clusters
519 T_1…T_6) for slow (top) and fast (bottom) spindles. **A)** Observed percentages for each channel cluster out of the
520 total number of slow or fast thalamic spindles, respectively. **B)** Difference of observed percentages from
521 permuted data for thalamic spindle co-occurrences. Positive values demarcate when observed data are more
522 likely to occur than by chance, negative values less likely than by chance. **C)** T_2 and T_3 spindles further subdivided
523 into unilateral and bilateral slow and fast thalamic spindles. The difference of observed and permuted data is
524 shown. Bars depict the group average, dots the individual participant data. Individual datapoints are
525 systematically offset so that horizontal order corresponds to participants 1 to 7. Filled in dots are significantly
526 different from permuted data at the within-participant level at $p < 0.05$ (two-sided), open dots depict data points
527 failing to meet significance at the within-participant level. The asterisks mark differences significant at $p < 0.05$
528 in the RMANOVA (corrected for multiple comparisons), brackets stand for differences between means, forking
529 out brackets for differences between individual bars.
530
531
532 *Multi- (but not single-) channel thalamic spindles show above-chance cortical counterparts*
533 Next, we investigated whether observed thalamic spindle activity was systematically related to
534 cortical spindle activity. For this analysis, spindles were subdivided according to the extent of
535 thalamic involvement into T_1, unilateral $T_{>1}$ or bilateral $T_{>1}$ spindles. We then categorized whether
536 these spindles occurred solely in the thalamus (T spindles) or also had a cortical counterpart (TC
537 spindles). We compared the occurrences of each spindle scenario to the total number of recorded
538 spindles, rather than the total number of thalamic spindles, which was the case in the analysis up
539 until now. Figure 6 shows the observed spindle percentages (A), and the difference between
540 observed and permuted data (B), both for slow and fast spindles in the top and bottom row,
541 respectively.
542 T and TC spindles were more or less likely than in the permuted data, depending on whether they
543 occurred in one channel or were unilateral or bilateral ($F_{1.04,6.24} = 24.74$; $p = 0.002$ in RMANOVA).
544 While most observed slow and fast spindles involving the thalamus were T_1 or T_1C spindles (fig.
545 6A, most leftward bars), these types of spindles were less likely than expected by chance (cf. 6B,
546 most leftward bars have negative values). Unilateral $T_{>1}$ (3.87 %; 95 % CI, 1.70 to 6.05) and $T_{>1}$C
547 (5.12 %; 95 % CI, 3.73 to 6.51) spindles were more likely to occur than expected by chance. In
548 contrast, bilateral $T_{>1}$ spindles occurred less often than predicted (-2.0 %; 95 % CI, -2.80 to -1.20),

549 whereas bilateral $T_{>1}C$ spindles occurred more often than predicted (2.96 %; 95 % CI, 1.30 to 4.67).
550 These observations did not differ between slow and fast spindles ($F_{1.03,6.18}$ = 0.62; p = 0.46 in
551 RMANOVA).
552 Except for bilateral $T_{>1}$ spindles without a cortical counterpart, spindles spanning more than one
553 thalamic channel were more likely to occur than expected by chance. These multichannel spindles
554 were also more likely to co-occur with cortical spindles. This can be seen in figure 6B, when looking
555 at the unilateral and bilateral spindles (middle left and middle right bars). These results suggest
556 that spindles at the thalamic (except for bilateral $T_{>1}$ spindles) and thalamocortical level tend to
557 co-occur across multiple channels systematically, indicating coordinated spindle activity.
558 We separately confirmed the absence of a systematic temporal offset between thalamic and
559 cortical spindles (supplementary material & suppl. fig. 3). A temporal shift would bias analyses of
560 spatiotemporal spindle overlap toward channel pairs with a smaller temporal offset, but this was
561 not the case.
562
563 *Not all cortical spindles have an anterior thalamic counterpart*
564 The data in the present study were recorded from a subsection of the thalamus and may have only
565 captured a subsample of spindles occurring in the thalamus. Because cortical spindles are thought
566 to depend on thalamic spindles and, more specifically, the projections of the different thalamic
567 nuclei to distinct cortical networks, our data may also contain cortical spindles that did not have a
568 thalamic counterpart (T_0C spindles). To test this, we counted the occurrences of cortical-only
569 spindles out of all recorded spindles, and compared them to permuted data. The most rightward
570 bar in each panel of figure 6 shows the percentage of these T_0C spindles. Indeed, in the observed
571 data (fig. 6A), around half of observed cortical EEG spindles did not have a thalamic counterpart
572 (slow: 41.46 ± 4.12 %; fast: 53.0 ± 9.04 %). This observation was higher than expected by chance
573 (slow: 14.38 ± 4.60 %; fast: 8.88 ± 3.74 %), but did not differ between slow and fast spindles (t(6)
574 = 1.87; p = 0.11). It may be that these T_0C spindles had counterparts in thalamic subparts not
575 sampled in our setup, such as more posterior nuclei.

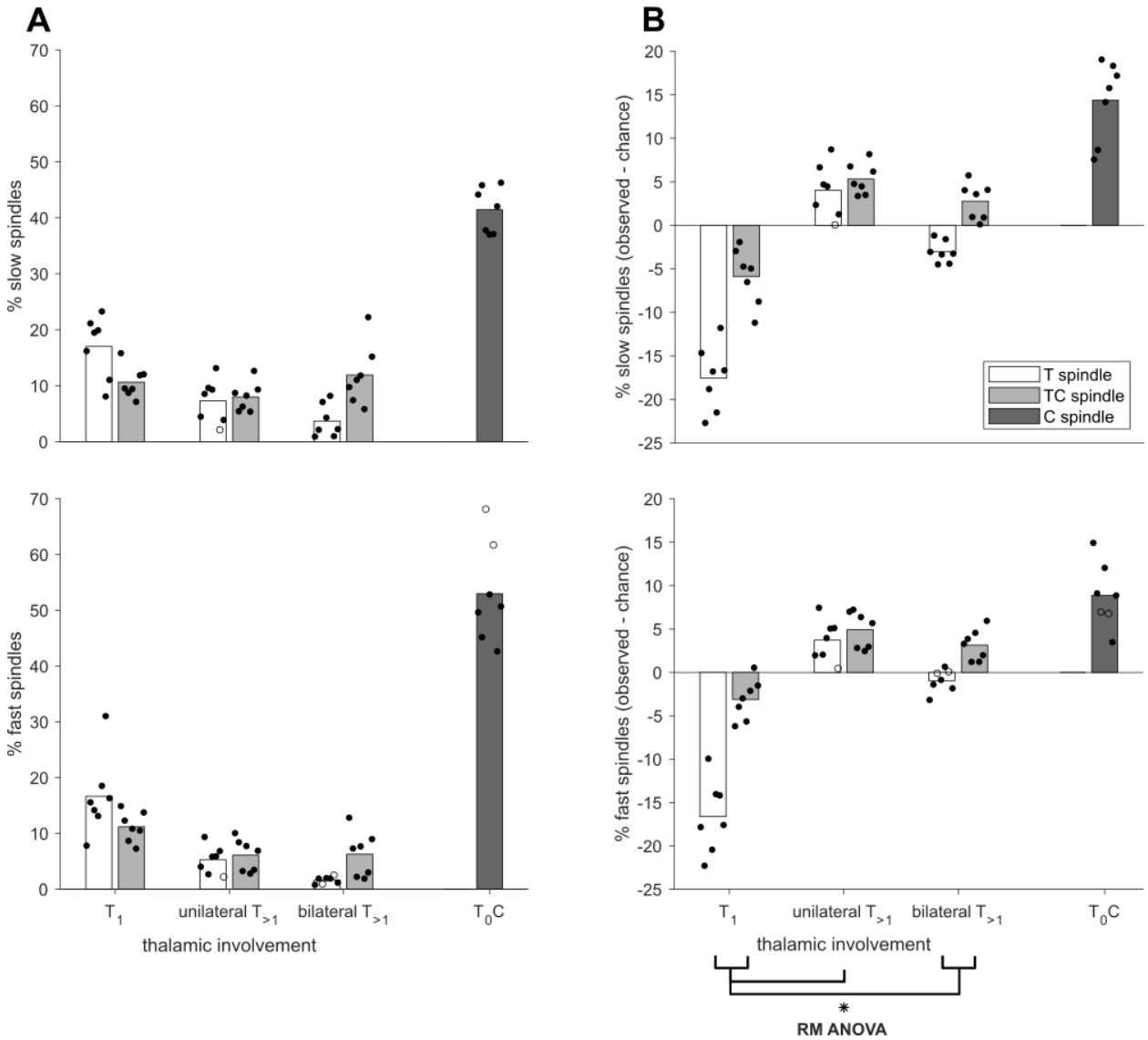

576

577 **Figure 6.** Observed spindles in thalamus and cortex, subdivided according to the level of involvement in the
578 thalamus (T_1 spindles or $T_{>1}$ spindles, unilateral and bilateral), and whether they were accompanied by a cortical
579 spindle (TC spindle, light grey) or not (T spindle, white). Cortical spindles without thalamic counterparts are also
580 shown (T_0C spindles, dark grey). **A)** Observation of each scenario as a percentage of the total number of slow
581 (top) and fast (bottom) spindles. **B)** Difference of observed from permuted percentages for slow (top) and fast
582 (bottom) spindles. Bars depict the group average, dots the individual participant data. Individual datapoints are
583 systematically offset so that horizontal order corresponds to participants 1 to 7. Filled in dots are significantly
584 different from permuted data at the within-participant level at $p < 0.05$ (two-sided), open dots depict data points
585 failing to meet significance at the within-participant level. The asterisks mark differences significant at $p < 0.05$
586 in the RMANOVA (corrected for multiple comparisons), brackets stand for differences between means, forking

587 out brackets for differences between individual bars. Note that there was no difference between slow and fast
588 spindles.
589
590 *Patterns of thalamocortical spindle overlap depend on level of thalamic involvement and spindle*
591 *subtypes*
592 Lastly, we investigated cortical topographies of spindles dependent on the type of thalamic spindle
593 and thalamic channel involvement. If coordinated thalamocortical spindle activity were to support
594 targeted engagement of thalamocortical networks, different cortical spindle topographies should
595 be observed based on different thalamic spindle properties. To compare differences in topography
596 for thalamocortical spindles, depending on the spindle type (slow vs. fast) and the level of thalamic
597 involvement (T_1C, unilateral $T_{>1}C$ or bilateral $T_{>1}C$ spindles), we computed the thalamocortical
598 overlap between all thalamic and cortical channel pairs across participants. The overlap quantifies
599 the percentage of data points during which two channels (here, a seed channel in the thalamus
600 and a target cortical channel) show simultaneous spindle activity. Since we verified that
601 thalamocortical spindle onset occurred predominantly simultaneously (suppl. fig. 3), this analysis
602 was carried out at 0-lag.
603 Figure 7 shows the median group difference of observed from permuted data for each category.
604 The median group data were calculated based on the individual data that differed significantly
605 from chance levels. The resulting topographies do not depict overlap in the left- and right
606 hemisphere, but rather contra- or ipsilateral to the thalamic source, respectively, because data
607 were averaged across participants, thalamus channels and hemispheres. Visual inspection
608 suggests that thalamocortical overlap for slow spindles had a frontal topography (fig. 7 A-C), and
609 fast spindles had a more central topography (fig. 7 D-F). Furthermore, the topographies seem to
610 progress from lateralized to more widespread as more thalamic channels were involved in a
611 thalamocortical spindle, which can be seen when comparing T_1C (fig. 7 A & D) to unilateral (fig. 7
612 B&E) and bilateral (fig. 7 C&F) $T_{>1}C$ spindles, respectively.
613 To summarize these different topographies, we computed the Center of Gravity (CoG), which
614 provides the spatial average weighted by the value of overlap at each cortical position. The CoG is
615 marked with a cross in each panel of figure 7. Note, that the CoG does not necessarily exactly

match the location suggested by the color scheme, given the different ways of calculating CoG and interpolating the colored surface.

For statistical analysis, we split the CoG into its x- and y-position allowing for quantifying the thalamocortical overlap's lateralization and shift along the anterior/posterior (a/p) axis relative to a central scalp EEG topography (Cz). We used bootstrapping to statistically evaluate the differences in CoG between conditions. Figure 8 shows the bootstrapped CoG data for lateralization (fig. 8 A-D) and a/p-shift (fig. 8 E-H), split into the different conditions of thalamic involvement and spindle type (slow spindles in blue, fast spindles in orange).

Lateralization of spindles (fig. 8 A-C) was significantly different from 0 for slow T_1C (0.055 ± 0.025; p = 0.001), slow unilateral $T_{>1}C$ (0.046 ± 0.02; p = 0.004), and fast T_1C (0.045 ± 0.012; p = 0) spindles, indicating that the average thalamocortical overlap for these conditions tended to be focused ipsilateral to the thalamic spindles. Slow bilateral $T_{>1}C$ (0.008 ± 0.013; p = 0.224), as well as fast unilateral $T_{>1}C$ (0.055 ± 0.034; p = 0.095) and fast bilateral $T_{>1}C$ (0.01 ± 0.013; p = 0.19) spindles were not significantly lateralized. A/p-shift was significantly different from 0 for slow T_1C (0.137 ± 0.029; p = 0), slow unilateral $T_{>1}C$ (0.075 ± 0.024; p = 0), and slow bilateral $T_{>1}C$ (0.108 ± 0.022; p = 0) spindles. Thus, the average CoG of thalamocortical spindle overlap of slow spindles was shifted anteriorly while fast T_1C (0.018 ± 0.015; p = 0.102), fast unilateral $T_{>1}C$ (0.018 ± 0.028; p = 0.198) and fast bilateral $T_{>1}C$ spindles (0.004 ± 0.03; p = 0.471) were not shifted along the a/p axis.

When comparing slow and fast spindles, T_1C slow spindles were significantly more anterior than T_1C fast spindles (0.12 ± 0.033; p = 0) but equally lateralized (0.009 ± 0.028; p = 0.355). Slow and fast unilateral $T_{>1}C$ spindles did not differ in terms of lateralization (-0.009 ± 0.039; p = 0.585) or shift on the anterior/posterior axis (0.056 ± 0.037; p = 0.076). Slow bilateral $T_{>1}C$ spindles were significantly more anterior than fast bilateral $T_{>1}C$ spindles (0.106 ± 0.039; p = 0.008), but did not differ in their lateralization (-0.002 ± 0.018; p = 0.556).

These results point towards differences in thalamocortical overlap depending on the spindle type (slow vs. fast) and level of thalamic involvement. As such, we observed that slow spindles tended to co-occur with cortical slow spindles in frontal scalp EEG sites. Co-occurrence of thalamic and cortical fast spindles was distributed more widely across the cortex, which was reflected by a more centralized average of thalamocortical overlap. Additionally, the level of involvement of the

thalamus in spindles was related to the cortical lateralization of thalamocortical overlap: During T_1C spindles and slow unilateral $T_{>1}C$ spindles, cortical electrodes ipsilateral to the thalamus channel(s) tended to engage in spindles together, whereas bilateral $T_{>1}C$ spindles showed a higher overlap with bilateral cortical electrodes.

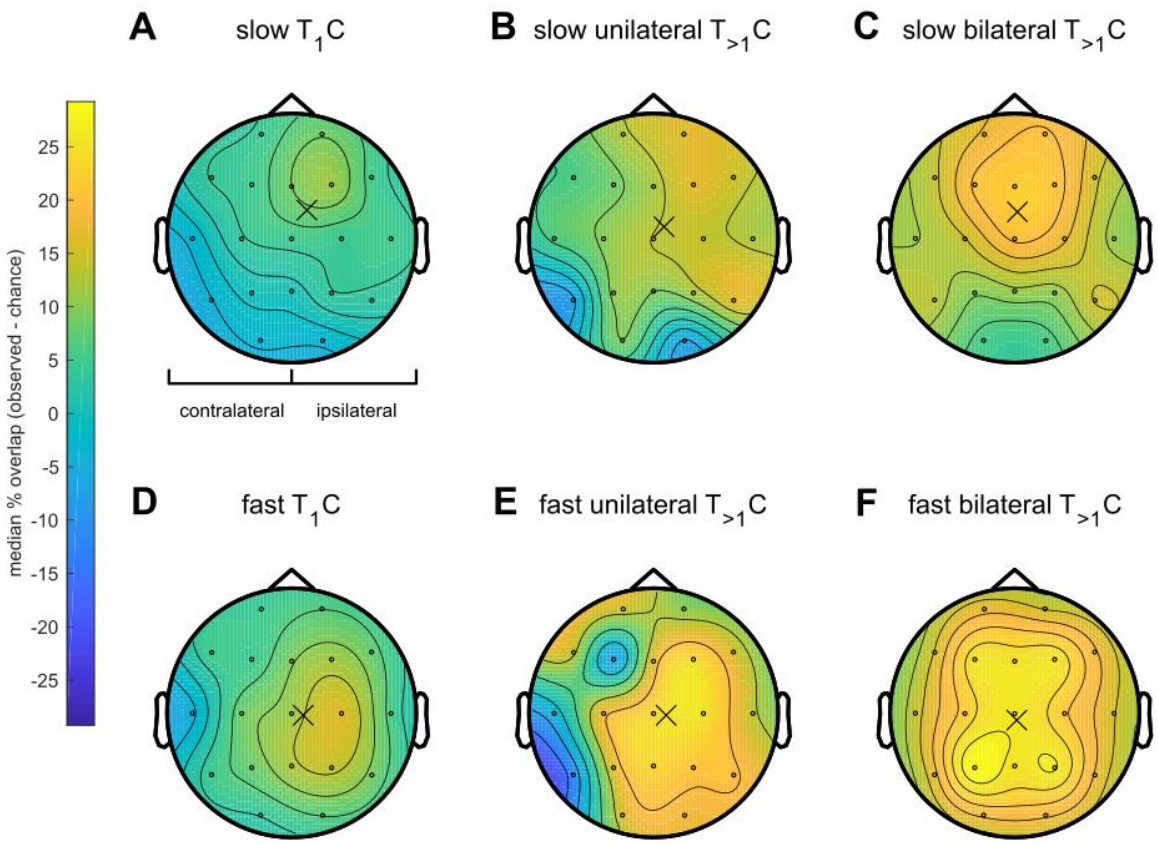

Figure 7. Thalamocortical spindle topographies. The difference of observed and permuted temporal overlap is shown as the group median. Accordingly, positive values describe a higher than by chance overlap, negative values a lower than by chance overlap. Data are averaged across thalamic channels, participants and hemispheres, such that values on the left within each topoplot describe the intensity of overlap contralateral and values on the right ipsilateral to the thalamus seed. The Center of Gravity is marked with a cross in each topoplot. Data are subdivided into spindle type and thalamic involvement: **A)** slow T_1C spindles; **B)** slow unilateral $T_{>1}C$ spindles; **C)** slow bilateral $T_{>1}C$ spindles; **D)** fast T_1C spindles; **E)** fast unilateral $T_{>1}C$ spindles; **F)** fast bilateral $T_{>1}C$ spindles.

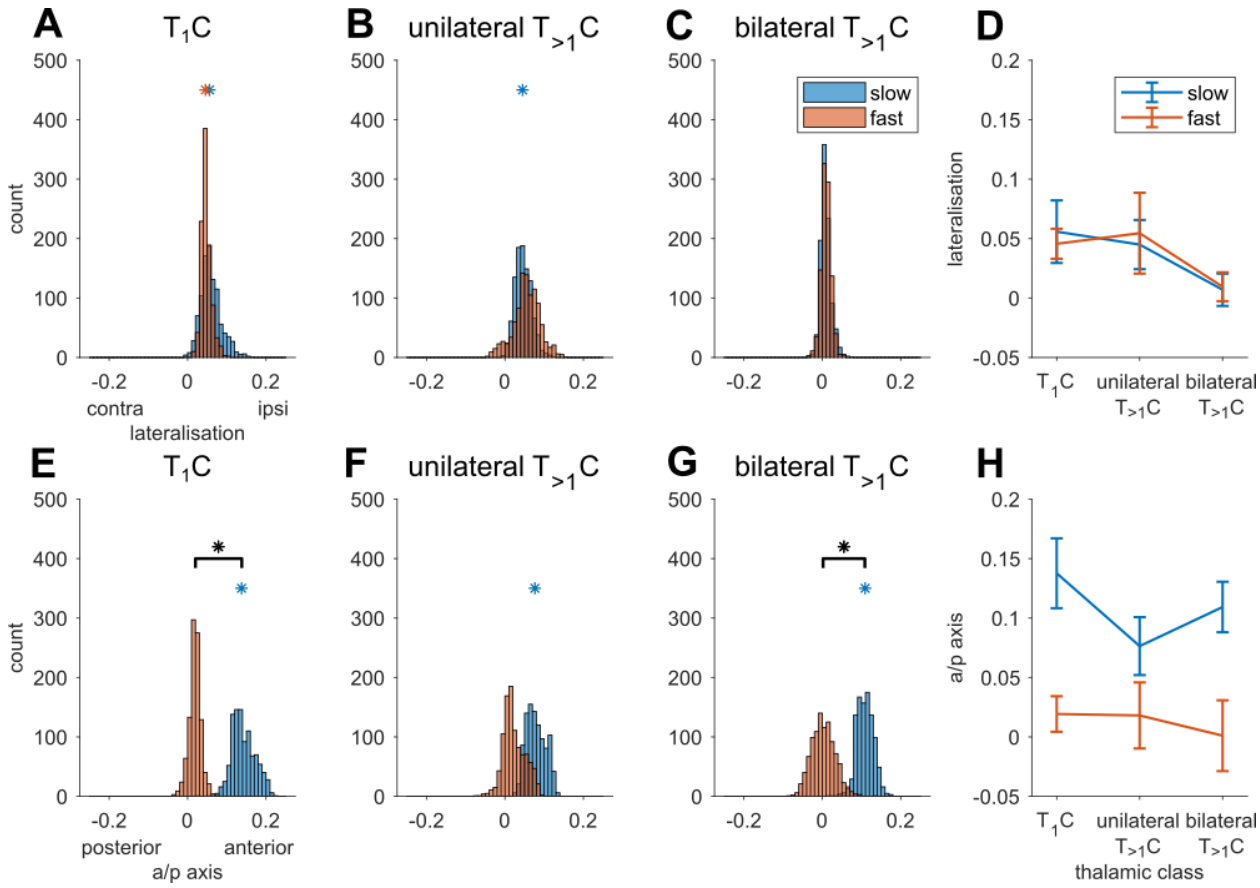

Figure 8. Center of Gravity of thalamocortical overlap, split into its x- and y-position, which describe lateralization and shift along the anterior/posterior (a/p) axis relative to electrode position Cz, respectively. Top row depicts the lateralization for **A)** T_1C spindles; **B)** unilateral $T_{>1}C$ spindles; **C)** bilateral $T_{>1}C$ spindles; **D)** median values and standard deviations of the distributions in A-C. Bottom row depicts a/p shift for **E)** T_1C spindles; **F)** unilateral $T_{>1}C$ spindles; **G)** bilateral $T_{>1}C$ spindles; **H)** median values and standard deviations of the distributions in E-G. Colored asterisks mark the distributions that differ from 0 at $p < 0.05$. Black asterisks and brackets mark distributions that differ from each other at $p < 0.05$.

Discussion

In the current study, we investigated the spatiotemporal coordination of spindles in the human anterior thalamus and cortex. Both slow and fast spindles were detected in the anterior thalamus, with a higher density of slow spindles. We categorized spindles based on their main frequency (slow vs. fast spindles) and level of thalamic involvement (spindles spanning one channel vs. multiple channels unilaterally vs. bilaterally) and compared observed patterns of spindle co-occurrence with permuted data. Figure 9 graphically summarizes predominant scenarios of thalamic and thalamocortical spindle (co-)occurrence we found in the permuted (A) and observed (B) data. We found that simultaneous multichannel spindle activity within thalamic and thalamocortical circuits occurred more often than expected by chance (fig. 9B). This points to spindle activity as a coordinated phenomenon across brain sites. Interestingly, multichannel spindles did not only co-occur unilaterally (fig. 9B.4&7), but also bilaterally within the thalamus (fig. 5; fig. 9B.5&6). When contrasting the different spindle subtypes based on their main frequency and the level of thalamic involvement, we observed similar rates of co-occurrence, but differences in the spatial pattern of cortical overlap (fig. 7). Overall, these results point to coordinated and differential patterns of sleep spindle co-occurrence in thalamocortical circuits.

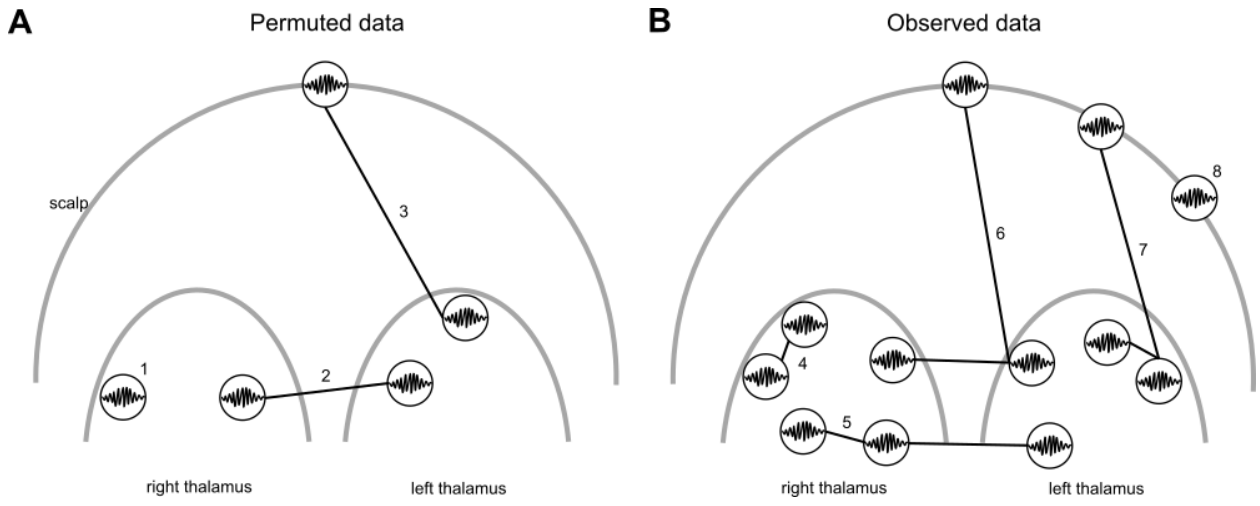

Figure 9. Graphical summary of thalamic and thalamocortical spindle (co-)occurrence, depicting spindle scenarios (numbered; cf. fig. 2 B) that appeared more often in the A) permuted or B) observed data. Bilateral thalamus and scalp are depicted schematically. Individual channels are indicated by circles, simultaneous spindle

activity is indicated by connecting lines. **A)** In the permuted data, locally restricted spindles predominated. Thalamic spindles were predominantly T_1 spindles (1) or bilateral T_2 spindles (2), and thalamocortical spindles mostly T_1C spindles (3). **B)** In the observed data, the most common spindle scenarios included two or more channels, indicating coordinated spindle activity. At the thalamic level, unilateral $T_{>1}$ spindles (4) predominated, as well as bilateral $T_{>2}$ spindles (5; here illustrated by a T_3 spindle). Thalamocortical spindles were predominantly bilateral $T_{>1}C$ (6) or unilateral $T_{>1}C$ spindles (7). There were also more cortical spindles without a thalamic counterpart (T_0C spindles; 8) than expected by chance.

There are alternative scenarios to coordinated and differentiated spindle activity across brain areas: For instance, spindles could be restricted to specific sites, which would preclude them from timing communication between brain areas during NREM sleep. Previous iEEG studies reported spindles as predominantly local in the cortex (Andrillon et al., 2011; Frauscher et al., 2015; Peter-Derex et al., 2012) and with low synchrony between cortical spindles and those in deeper brain structures like insula and hippocampus (Frauscher et al., 2015). These reports gave rise to the idea of sleep spindles as a local phenomenon. Although we observed many occurrences of spindles restricted to one channel, we also saw that spindles often spanned multiple channels, both at the thalamic (~50 % of spindles) and the thalamocortical level (~35% of all spindles engaged at least one thalamic and one cortical channel). Most of these multi-channel spindle scenarios occurred more often than predicted by chance, suggesting that spindle activity in thalamocortical networks is indeed coordinated rather than always being locally restricted. While we cannot exclude the possibility that some multichannel spindles in our data reflect volume conduction from a single source, volume conduction clearly cannot explain many of the patterns we observed, among which bilateral spindles picked up by electrodes in opposite hemispheres (cf. suppl.fig. 1C), or spindle onset and duration differences between neighbouring channels (cf. fig. 1C.I and II). Moreover, the proportion of multi-channel thalamic and thalamocortical spindles observed here, may be an underestimation as the exact thalamic recording sites differed between individuals, and consequently only sample a subsection of the thalamus. Events categorized here as T_1, T_1C or T_0C spindles may have engaged thalamic regions not sampled in our setup. Our findings thus indicate

718 that many spindles are not local, and do not co-occur merely by chance, but are coordinated over
719 wide areas of the thalamocortical network.

720 Although pathological brains differ from healthy ones, treatment with benzodiazepines and
721 anticonvulsant drugs may influence the sleep architecture (for a comprehensive review see Jain &
722 Glauser, 2014) and spindles (Leong et al., 2022; Plante et al., 2015) and the wide age range in our
723 sample may bias spindle-related characteristics (Muehlroth & Werkle-Bergner, 2020), clinical
724 populations are presently the only opportunity to directly measure time-resolved recordings of
725 the human thalamus. Previous studies have reported thalamocortical spindles in medial/anterior
726 thalamus and cortex (Schreiner, Kaufmann, et al., 2021; Szalárdy et al., 2021) as well as posterior
727 thalamus and cortex (Bastuji et al., 2020; Mak-McCully et al., 2017), albeit only one of these studies
728 investigated thalamic and thalamocortical spindle co-occurrence in a more systematic fashion
729 (Bastuji et al., 2020). In that study, around half of all thalamic spindles occurred in one channel
730 and the remaining half spread across two or more channels. These reports were limited to the
731 posterior thalamus due to clinical demands, were not contrasted with chance spindle co-
732 occurrence and only investigated fast spindles. Our data now add information on the anterior
733 thalamus.

734 In contrast to previous literature, which focused on fast spindles, we systematically investigated
735 thalamic and thalamocortical spindle co-occurrence separately for slow and fast spindles. In our
736 data, both spindle types were coordinated in a largely similar fashion, although some differences
737 were also found. Slow and fast spindles were more likely to span multiple channels in the observed
738 than permuted data, both unilaterally and bilaterally, and co-occurred between thalamus and
739 neocortex. Our time lag analysis revealed simultaneous activation of thalamic and cortical
740 spindles. The lack of temporal sequence in our data does not provide information on causal
741 relations of spindle activity across regions. However, our findings provide evidence that both slow
742 and fast spindles are present in the (anterior) thalamus, and that both engage in a coordinated
743 fashion with the neocortex. It is thus not likely that slow spindles are specific to cortico-cortico
744 interactions, as suggested previously (Mölle et al., 2011). Interestingly, slow and fast
745 thalamocortical spindles did show different topographical patterns of thalamocortical overlap:
746 slow thalamic spindles showed higher overlap with frontal scalp EEG electrodes, whereas fast

747 thalamic spindles showed higher overlap with centro-posterior scalp EEG electrodes. These
748 topographies of overlap are reminiscent of sites of slow and fast spindle activity observed in
749 previous (i)EEG studies (Andrillon et al., 2011; Mölle et al., 2011; Peter-Derex et al., 2012). Note,
750 however, that the different patterns we uncovered cannot be merely explained by the higher
751 density of slow spindles in frontal EEG channels (cf. fig. 3C). We used permutation testing to
752 control for the bias of higher spindle density/duration on spurious spindle overlap. Thus, although
753 the frequency-based spindle dichotomy has been criticized as overly simplified (Gonzalez et al.,
754 2021), our results suggest that thalamic spindles engage different cortical networks, depending
755 on their main frequency.

756 The topographical patterns of thalamocortical spindle overlap were not only related to the main
757 frequency of a given spindle, but also to the level of involvement of the thalamus. Andrillon and
758 colleagues (2011) reported that spindles occasionally span multiple channels across the cortex. In
759 this scenario, spindles travel along the cortical posterior-to-anterior axis (Andrillon et al., 2011;
760 Muller et al., 2016). In the present study, we observed that multi-channel thalamic spindles were
761 related to an increase in the number of cortical channels showing high thalamocortical spindle
762 overlap. Consequently, the different cortical spindle scenarios (localized vs. global cortical events)
763 reported in previous (i)EEG studies could be related to differential involvement of the thalamus in
764 these spindles. Accordingly, multichannel cortical spindles could arise as a consequence of
765 multichannel thalamic spindles. That is, when a spindle travels through the thalamus, this may be
766 reflected as a cortical traveling spindle mediated by thalamocortical projections with the engaged
767 thalamic sites. In fact, the patterns of thalamocortical spindle co-occurrence in our data (cf. fig. 7)
768 suggest that this might be the case. For instance, the thalamocortical overlap of fast spindle events
769 differed between spindles occurring in one thalamic channel and those spanning bilateral thalamic
770 channels: In the former case, the thalamocortical overlap was spatially restricted to centro-
771 posterior cortical sites ipsilateral to the thalamic site (cf. fig. 7 & 8), whereas in the latter case, the
772 overlap was more widespread across the cortex bilaterally. Interestingly, cross-hemispheric co-
773 occurrence of cortical spindles is preserved in callosotomized patients, suggesting that cortical
774 spindle spread may depend on thalamocortical instead of cortico-cortico connections (Bernardi et
775 al., 2021). The results of the present study add to the currently limited literature on

interhemispheric spindle co-occurrence by showing that cortical spread of spindle activity is related to the level of involvement of the thalamus. More broadly, the involvement of different thalamic sites in a spindle may engage different cortical networks.

Spindles may facilitate network communication during memory consolidation

Memory consolidation requires reactivation in hippocampo-cortical circuits to trigger structural changes (Josselyn et al., 2015). This reactivation must be specific to the neuronal populations involved in encoding the memory, and thus requires coordinated activity across (sub)cortical networks. Hippocampal ripples (80 – 140 Hz), which have been linked to memory reactivation (Zhang, Fell, & Axmacher, 2018), co-occur with spindles in the hippocampus and cortex (Ngo et al., 2020; Staresina et al., 2015), the anterior thalamus (Szalárdy et al., 2021) and in the anterior thalamus and hippocampus (Sarasso et al., 2014). Spindles are hypothesized to align windows of excitability in hippocampo-cortical circuits, and thereby coordinate the information transfer necessary for long term memory consolidation (Klinzing et al., 2019).

The thalamus is richly connected with cortical and subcortical structures (Cappe, Morel, Barone, & Rouiller, 2009; Jankowski et al., 2013; Zhang, Snyder, Shimony, Fox, & Raichle, 2010) and has been proposed as a connector hub between distinct cortical networks (Kawabata et al., 2021). Recent research hints at an active role of the thalamus in memory consolidation during sleep (Klinzing et al., 2019). According to this view, thalamus functions as a switchboard to enhance processing within and between specific cortical networks as required by task demands (Nakajima & Halassa, 2017; Schmitt et al., 2017). Those same mechanisms seem to be engaged during spindle generation in rodent NREM sleep (Chen et al., 2016; Halassa et al., 2014). Regarding memory reactivation, spindles in the thalamus (within or across thalamic nuclei) could selectively engage (sub)cortical sites through its rich projections. This could lead to carefully timed communication between the hippocampus and the cortical network(s) implicated in a specific memory and thereby enable reactivation of memory traces crucial for memory consolidation.

Previous studies have reported the importance of temporally (Latchoumane et al., 2017; Schreiner, Petzka, et al., 2021) and spatially (Petzka et al., 2022) organized cortical spindles during

804 memory consolidation processes. Although our study did not include a memory task, here we add
805 to this literature by showing that thalamocortical spindle activity is temporally coordinated and
806 spatially specific. Further research using memory tasks needs to be conducted to directly study
807 how the thalamocortical processes reported here may support memory consolidation.

808

809 *Conclusion*

810 The present study investigated (co-)occurrence of sleep spindles in the anterior thalamus and
811 neocortex. Up to half of the recorded spindles co-occurred across multiple channels, both at the
812 thalamic and thalamocortical level. Although spindles were more likely to engage the thalamus
813 unilaterally, we also observed simultaneous bilateral thalamic spindles. Slow and fast spindles
814 were observed in the anterior thalamus. Both slow and fast, as well as single channel and
815 multichannel thalamic spindles were associated with distinct topographical patterns of spindle co-
816 occurrence in the cortex. As such, slow thalamocortical spindles generally co-occurred with more
817 frontal scalp EEG channels, while fast thalamocortical spindles showed a wider cortical overlap,
818 averaging highest at central scalp EEG sites. Single channel and unilateral thalamic spindles had
819 more lateralized cortical co-occurrence patterns than bilateral thalamic spindles. These diverse
820 patterns of thalamocortical spindle co-occurrence could be involved in selective engagement of
821 thalamocortical networks during memory consolidation and other cognitive processes.

822

Acknowledgements: The authors would like to thank all patients and their families for the cooperation in this study. In addition, the authors would like to thank Julio Rodriguez Larios for providing helpful feedback, and the editors and reviewers who have dedicated their time to provide comments and questions which greatly improved this manuscript.

Competing Interests: The authors declare no competing interest.

Funding: This research was funded by an internal grant from the Centre for Integrative Neuroscience at Maastricht University.

Author Contributions

Hannah Bernhard: Conceptualization, Data curation, Formal analysis, Methodology, Project administration, Resources, Software, Validation, Visualization, Writing – original draft, Writing – review & editing. **Fred Schaper:** Data curation, Investigation, Project administration, Resources, Visualization, Writing – review & editing. **Marcus Janssen:** Investigation, Resources, Writing – review & editing. **Erik Gommer:** Data curation, Investigation, Project administration, Resources, Writing – review & editing. **Bernadette Jansma:** Funding acquisition, Supervision, Writing – review & editing. **Vivianne Van Kranen-Mastenbroek:** Funding acquisition, Investigation, Resources, Supervision, Writing – review & editing. **Rob Rouhl:** Funding Acquisition, Investigation, Project administration, Resources, Supervision, Writing – review & editing. **Peter de Weerd:** Conceptualization, Funding acquisition, Methodology, Resources, Supervision, Writing – original draft, Writing – review & editing. **Joel Reithler:** Conceptualization, Formal analysis, Methodology, Resources, Supervision, Validation, Visualization, Writing – original draft, Writing – review & editing. **Mark Roberts:** Conceptualization, Formal analysis, Funding acquisition, Methodology, Resources, Software, Supervision, Validation, Visualization, Writing – original draft, Writing – review & editing. **Louis Wagner:** Investigation, Resources. **Albert Colon:** Investigation, Resources. **Danny Hilkman:** Investigation, Resources. **Marielle Vlooswijk:** Investigation, Resources. **Jeske Nelissen:** Investigation, Resources. **Linda Ackermans:** Investigation, Resources. **Yasin Temel:** Investigation, Resources.

References

Aggleton, J. P., O'Mara, S. M., Vann, S. D., Wright, N. F., Tsanov, M., & Erichsen, J. T. (2010). Hippocampal-anterior thalamic pathways for memory: uncovering a network of direct and indirect actions. *European Journal of Neuroscience*, *31*(12), 2292–2307. https://doi.org/10.1111/j.1460-9568.2010.07251.x

Andrillon, T., & Kouider, S. (2020). The vigilant sleeper: neural mechanisms of sensory (de)coupling during sleep. In *Current Opinion in Physiology* (Vol. 15, pp. 47–59). Elsevier Ltd. https://doi.org/10.1016/j.cophys.2019.12.002

Andrillon, T., Nir, Y., Staba, R. J., Ferrarelli, F., Cirelli, C., Tononi, G., & Fried, I. (2011). Sleep spindles in humans: Insights from intracranial EEG and unit recordings. *Journal of Neuroscience*, *31*(49), 17821–17834. https://doi.org/10.1523/JNEUROSCI.2604-11.2011

Avants, B. B., Epstein, C. L., Grossman, M., & Gee, J. C. (2008). Symmetric diffeomorphic image registration with cross-correlation: Evaluating automated labeling of elderly and neurodegenerative brain. *Medical Image Analysis*, *12*, 26–41. https://doi.org/10.1016/J.MEDIA.2007.06.004

Bastuji, H., Lamouroux, P., Villalba, M., Magnin, M., & Garcia-Larrea, L. (2020). Local sleep spindles in the human thalamus. *The Journal of Physiology*, JP279045. https://doi.org/10.1113/JP279045

Bernardi, G., Avvenuti, G., Cataldi, J., Lattanzi, S., Ricciardi, E., Polonara, G., Silvestrini, M., Siclari, F., Fabri, M., & Bellesi, M. (2021). Role of corpus callosum in sleep spindle synchronization and coupling with slow waves. *Brain Communications*, *3*(2), 1–14. https://doi.org/10.1093/braincomms/fcab108

Berry, R. B., Brooks, R., Gamaldo, C. E., Harding, S. M., Lloyd, R. M., & Marcus, C. L. (2015). American Academy of Sleep Medicine. The AASM Manual for the Scoring of Sleep and Associated Events : Rules, Terminology, and Technical Specifications, Version 2.2. *American Academy of Sleep*.

Cappe, C., Morel, A., Barone, P., & Rouiller, E. M. (2009). The Thalamocortical Projection Systems in Primate: An Anatomical Support for Multisensory and Sensorimotor Interplay. *Cerebral Cortex*, *19*(9), 2025–2037. https://doi.org/10.1093/cercor/bhn228

Chen, Z., Wimmer, R. D., Wilson, M. A., & Halassa, M. M. (2016). Thalamic Circuit Mechanisms Link Sensory Processing in Sleep and Attention. *Frontiers in Neural Circuits*, *9*, 83. https://doi.org/10.3389/fncir.2015.00083

Feldmann, L. K., Neumann, W. J., Faust, K., Schneider, G. H., & Kühn, A. A. (2021). Risk of Infection after Deep Brain Stimulation Surgery with Externalization and Local-Field Potential Recordings: Twelve-Year Experience from a Single Institution. *Stereotactic and Functional Neurosurgery*, *99*(6), 512–520. https://doi.org/10.1159/000516150

Fernandez, L. M. J., & Lüthi, A. (2020). Sleep spindles: Mechanisms and functions. *Physiological Reviews*, *100*(2), 805–868. https://doi.org/10.1152/PHYSREV.00042.2018/ASSET/IMAGES/LARGE/Z9J0022029380013.JPEG

Fisher, R., Salanova, V., Witt, T., Worth, R., Henry, T., Gross, R., Oommen, K., Osorio, I., Nazzaro, J., Labar, D., Kaplitt, M., Sperling, M., Sandok, E., Neal, J., Handforth, A., Stern, J., DeSalles, A., Chung, S., Shetter, A., … Young, C. (2010). Electrical stimulation of the anterior nucleus of thalamus for treatment of refractory epilepsy. *Epilepsia*, *51*(5), 899–908. https://doi.org/10.1111/J.1528-1167.2010.02536.X

Fonov, V., Evans, A. C., Botteron, K., Almli, C. R., McKinstry, R. C., Collins, D. L., & Brain Development Cooperative Group. (2011). Unbiased Average Age-Appropriate Atlases for Pediatric Studies. *NeuroImage*, *54*, 313. https://doi.org/10.1016/J.NEUROIMAGE.2010.07.033

Frauscher, B., von Ellenrieder, N., Dubeau, F., & Gotman, J. (2015). Scalp spindles are associated with widespread intracranial activity with unexpectedly low synchrony. *NeuroImage*, *105*, 1–12. https://doi.org/10.1016/J.NEUROIMAGE.2014.10.048

Friston, K. J., Holmes, A. P., Worsley, K. J., Poline, J. -P, Frith, C. D., & Frackowiak, R. S. J. (1994).

Statistical parametric maps in functional imaging: A general linear approach. *Human Brain Mapping*, *2*(4), 189–210. https://doi.org/10.1002/HBM.460020402

Frost, B. E., Martin, S. K., Cafalchio, M., Islam, M. N., Aggleton, J. P., & O'Mara, S. M. (2021). Anterior Thalamic Inputs are Required for Subiculum Spatial Coding, with Associated Consequences for Hippocampal Spatial Memory. *The Journal of Neuroscience*, JN-RM-2868-20. https://doi.org/10.1523/JNEUROSCI.2868-20.2021

Gonzalez, C., Jiang, X., Gonzalez-Martinez, J., & Halgren, E. (2021). Human spindle variability. *BioRxiv*, 2021.09.02.458632. https://doi.org/10.1101/2021.09.02.458632

Halassa, M. M., Chen, Z., Wimmer, R. D., Brunetti, P. M., Zhao, S., Zikopoulos, B., Wang, F., Brown, E. N., & Wilson, M. A. (2014). State-Dependent Architecture of Thalamic Reticular Subnetworks. *Cell*, *158*(4), 808–821. https://doi.org/10.1016/J.CELL.2014.06.025

Horn, A., Li, N., Dembek, T. A., Kappel, A., Boulay, C., Ewert, S., Tietze, A., Husch, A., Perera, T., Neumann, W. J., Reisert, M., Si, H., Oostenveld, R., Rorden, C., Yeh, F. C., Fang, Q., Herrington, T. M., Vorwerk, J., & Kühn, A. A. (2019). Lead-DBS v2: Towards a comprehensive pipeline for deep brain stimulation imaging. *NeuroImage*, *184*, 293–316. https://doi.org/10.1016/J.NEUROIMAGE.2018.08.068

Horn, A., Reich, M., Vorwerk, J., Li, N., Wenzel, G., Fang, Q., Schmitz-Hübsch, T., Nickl, R., Kupsch, A., Volkmann, J., Kühn, A. A., & Fox, M. D. (2017). Connectivity Predicts deep brain stimulation outcome in Parkinson disease. *Annals of Neurology*, *82*, 67–78. https://doi.org/10.1002/ANA.24974

Jain, S. V., & Glauser, T. A. (2014). Effects of epilepsy treatments on sleep architecture and daytime sleepiness: An evidence-based review of objective sleep metrics. *Epilepsia*, *55*(1), 26–37. https://doi.org/10.1111/EPI.12478

Jankowski, M. M., Ronnqvist, K. C., Tsanov, M., Vann, S. D., Wright, N. F., Erichsen, J. T., Aggleton, J. P., & O'Mara, S. M. (2013). The anterior thalamus provides a subcortical circuit supporting memory and spatial navigation. *Frontiers in Systems Neuroscience*, *7*, 45. https://doi.org/10.3389/fnsys.2013.00045

930 Josselyn, S. A., Köhler, S., & Frankland, P. W. (2015). Finding the engram. *Nature Reviews*
931 *Neuroscience*, *16*(9), 521–534. https://doi.org/10.1038/nrn4000

932 Kawabata, K., Bagarinao, E., Watanabe, H., Maesawa, S., Mori, D., Hara, K., Ohdake, R., Masuda,
933 M., Ogura, A., Kato, T., Koyama, S., Katsuno, M., Wakabayashi, T., Kuzuya, M., Hoshiyama,
934 M., Isoda, H., Naganawa, S., Ozaki, N., & Sobue, G. (2021). Bridging large-scale cortical
935 networks: Integrative and function-specific hubs in the thalamus. *IScience*, *24*(10), 103106.
936 https://doi.org/10.1016/J.ISCI.2021.103106

937 Klinzing, J. G., Niethard, N., & Born, J. (2019). Mechanisms of systems memory consolidation
938 during sleep. *Nature Neuroscience*, 1–13. https://doi.org/10.1038/s41593-019-0467-3

939 Latchoumane, C.-F. V., Ngo, H.-V. V., Born, J., & Shin, H.-S. (2017). Thalamic Spindles Promote
940 Memory Formation during Sleep through Triple Phase-Locking of Cortical, Thalamic, and
941 Hippocampal Rhythms. *Neuron*, *95*(2), 424-435.e6.
942 https://doi.org/10.1016/J.NEURON.2017.06.025

943 Lehtimäki, K., Coenen, V. A., Gonçalves Ferreira, A., Boon, P., Elger, C., Taylor, R. S., Ryvlin, P., Gil-
944 Nagel, A., Gielen, F., Brionne, T. C., Abouihia, A., & Beth, G. (2019). The Surgical Approach to
945 the Anterior Nucleus of Thalamus in Patients With Refractory Epilepsy: Experience from the
946 International Multicenter Registry (MORE). *Neurosurgery*, *84*(1), 141–150.
947 https://doi.org/10.1093/NEUROS/NYY023

948 Leong, C. W. Y., Leow, J. W. S., Grunstein, R. R., Naismith, S. L., Teh, J. Z., D'Rozario, A. L., & Saini,
949 B. (2022). A systematic scoping review of the effects of central nervous system active drugs
950 on sleep spindles and sleep-dependent memory consolidation. *Sleep Medicine Reviews*, *62*,
951 101605. https://doi.org/10.1016/J.SMRV.2022.101605

952 Mak-McCully, R. A., Rolland, M., Sargsyan, A., Gonzalez, C., Magnin, M., Chauvel, P., Rey, M.,
953 Bastuji, H., & Halgren, E. (2017). Coordination of cortical and thalamic activity during non-
954 REM sleep in humans. *Nature Communications*, *8*(1), 15499.
955 https://doi.org/10.1038/ncomms15499

956 Mölle, M., Bergmann, T. O., Marshall, L., & Born, J. (2011). Fast and Slow Spindles during the

Sleep Slow Oscillation: Disparate Coalescence and Engagement in Memory Processing. *Sleep*, *34*(10), 1411–1421. https://doi.org/10.5665/SLEEP.1290

Muehlroth, B. E., & Werkle-Bergner, M. (2020). Understanding the interplay of sleep and aging: Methodological challenges. *Psychophysiology*, *57*(3), e13523. https://doi.org/10.1111/psyp.13523

Muller, L., Piantoni, G., Koller, D., Cash, S. S., Halgren, E., & Sejnowski, T. J. (2016). Rotating waves during human sleep spindles organize global patterns of activity that repeat precisely through the night. *ELife*, *5*, 1–16. https://doi.org/10.7554/elife.17267

Nakajima, M., & Halassa, M. M. (2017). Thalamic control of functional cortical connectivity. *Current Opinion in Neurobiology*, *44*, 127–131. https://doi.org/10.1016/J.CONB.2017.04.001

Ngo, H.-V., Fell, J., & Staresina, B. (2020). Sleep spindles mediate hippocampal-neocortical coupling during long-duration ripples. *ELife*. https://doi.org/10.7554/eLife.57011

Ngo, H.-V., Martinetz, T., Born, J., & Mölle, M. (2013). Auditory Closed-Loop Stimulation of the Sleep Slow Oscillation Enhances Memory. *Neuron*, *78*(3), 545–553. https://doi.org/10.1016/J.NEURON.2013.03.006

Oostenveld, R., Fries, P., Maris, E., & Schoffelen, J.-M. (2011). FieldTrip: Open Source Software for Advanced Analysis of MEG, EEG, and Invasive Electrophysiological Data. *Computational Intelligence and Neuroscience*, *2011*, 1–9. https://doi.org/10.1155/2011/156869

Peter-Derex, L., Comte, J. C., Mauguière, F., & Salin, P. A. (2012). Density and frequency caudo-rostral gradients of sleep spindles recorded in the human cortex. *Sleep*, *35*(1), 69–79. https://doi.org/10.5665/sleep.1588

Petzka, M., Chatburn, A., Charest, I., Balanos, G. M., & Staresina, B. P. (2022). Sleep spindles track cortical learning patterns for memory consolidation. *Current Biology*, *32*(11), 2349-2356.e4. https://doi.org/10.1016/J.CUB.2022.04.045

Plante, D. T., Goldstein, M. R., Cook, J. D., Smith, R., Riedner, B. A., Rumble, M. E., Jelenchick, L., Roth, A., Tononi, G., Benca, R. M., & Peterson, M. J. (2015). Effects of oral temazepam on

983 sleep spindles during non-rapid eye movement sleep: A high-density EEG investigation.
984 *European Neuropsychopharmacology : The Journal of the European College of*
985 *Neuropsychopharmacology*, *25*(10), 1600–1610.
986 https://doi.org/10.1016/J.EURONEURO.2015.06.005

987 Salanova, V., Witt, T., Worth, R., Henry, T. R., Gross, R. E., Nazzaro, J. M., Labar, D., Sperling, M.
988 R., Sharan, A., Sandok, E., Handforth, A., Stern, J. M., Chung, S., Henderson, J. M., French, J.,
989 Baltuch, G., Rosenfeld, W. E., Garcia, P., Barbaro, N. M., … Fisher, R. (2015). Long-term
990 efficacy and safety of thalamic stimulation for drug-resistant partial epilepsy. *Neurology*,
991 *84*(10), 1017. https://doi.org/10.1212/WNL.0000000000001334

992 Sarasso, S., Proserpio, P., Pigorini, A., Moroni, F., Ferrara, M., De Gennaro, L., De Carli, F., Lo
993 Russo, G., Massimini, M., & Nobili, L. (2014). Hippocampal sleep spindles preceding
994 neocortical sleep onset in humans. *NeuroImage*, *86*, 425–432.
995 https://doi.org/10.1016/J.NEUROIMAGE.2013.10.031

996 Schaper, F. L., Plantinga, B. R., Colon, A. J., Wagner, G. L., Boon, P., Blom, N., Gommer, E. D.,
997 Hoogland, G., Ackermans, L., Rouhl, R. P., & Temel, Y. (2020). Deep Brain Stimulation in
998 Epilepsy: A Role for Modulation of the Mammillothalamic Tract in Seizure Control?
999 *Neurosurgery*, *87*(3), 602–610. https://doi.org/10.1093/neuros/nyaa141

1000 Schaper, F. L., Zhao, Y., Janssen, M. L., Wagner, G., Colon, A. J., Hilkman, D. M., Gommer, E.,
1001 Vlooswijk, M. C., Hoogland, G., Ackermans, L., Bour, L. J., Van Wezel, R. J., Boon, P., Temel,
1002 Y., Heida, T., Van Kranen-Mastenbroek, V. H., & Rouhl, R. P. (2019). Single-Cell Recordings to
1003 Target the Anterior Nucleus of the Thalamus in Deep Brain Stimulation for Patients with
1004 Refractory Epilepsy. *International Journal of Neural Systems*, *11*.
1005 https://doi.org/10.1142/S0129065718500120

1006 Schmitt, L. I., Wimmer, R. D., Nakajima, M., Happ, M., Mofakham, S., & Halassa, M. M. (2017).
1007 Thalamic amplification of cortical connectivity sustains attentional control. *Nature*,
1008 *545*(7653), 219–223. https://doi.org/10.1038/nature22073

1009 Schönecker, T., Kupsch, A., Kühn, A. A., Schneider, G. H., & Hoffmann, K. T. (2009). Automated

1010 optimization of subcortical cerebral MR imaging-atlas coregistration for improved
1011 postoperative electrode localization in deep brain stimulation. *American Journal of*
1012 *Neuroradiology*, *30*(10), 1914–1921. https://doi.org/10.3174/AJNR.A1741

1013 Schreiner, T., Kaufmann, E., Noachtar, S., Mehrkens, J.-H., & Staudigl, T. (2021). The human
1014 thalamus orchestrates neocortical oscillations during NREM sleep. *BioRxiv*,
1015 2021.12.11.471766. https://doi.org/10.1101/2021.12.11.471766

1016 Schreiner, T., Petzka, M., Staudigl, T., & Staresina, B. P. (2021). Endogenous memory reactivation
1017 during sleep in humans is clocked by slow oscillation-spindle complexes. *Nature*
1018 *Communications*, *12*(1), 3112. https://doi.org/10.1038/s41467-021-23520-2

1019 Staresina, B. P., Bergmann, T. O., Bonnefond, M., van der Meij, R., Jensen, O., Deuker, L., Elger, C.
1020 E., Axmacher, N., & Fell, J. (2015). Hierarchical nesting of slow oscillations, spindles and
1021 ripples in the human hippocampus during sleep. *Nature Neuroscience*, *18*(11), 1679–1686.
1022 https://doi.org/10.1038/nn.4119

1023 Su, J. H., Thomas, F. T., Kasoff, W. S., Tourdias, T., Choi, E. Y., Rutt, B. K., & Saranathan, M. (2019).
1024 Thalamus Optimized Multi Atlas Segmentation (THOMAS): fast, fully automated
1025 segmentation of thalamic nuclei from structural MRI. *NeuroImage*, *194*, 272–282.
1026 https://doi.org/10.1016/J.NEUROIMAGE.2019.03.021

1027 Sweeney-Reed, C. M., Buentjen, L., Voges, J., Schmitt, F. C., Zaehle, T., Kam, J. W. Y., Kaufmann,
1028 J., Heinze, H. J., Hinrichs, H., Knight, R. T., & Rugg, M. D. (2021). The role of the anterior
1029 nuclei of the thalamus in human memory processing. *Neuroscience & Biobehavioral*
1030 *Reviews*, *126*, 146–158. https://doi.org/10.1016/J.NEUBIOREV.2021.02.046

1031 Sweeney-Reed, C. M., Zaehle, T., Voges, J., Schmitt, F. C., Buentjen, L., Borchardt, V., Walter, M.,
1032 Hinrichs, H., Heinze, H.-J., Rugg, M. D., & Knight, R. T. (2017). Anterior Thalamic High
1033 Frequency Band Activity Is Coupled with Theta Oscillations at Rest. *Frontiers in Human*
1034 *Neuroscience*, *11*(July), 1–13. https://doi.org/10.3389/fnhum.2017.00358

1035 Sweeney-Reed, C. M., Zaehle, T., Voges, J., Schmitt, F. C., Buentjen, L., Kopitzki, K., Esslinger, C.,
1036 Hinrichs, H., Heinze, H. J., Knight, R. T., & Richardson-Klavehn, A. (2014). Corticothalamic

phase synchrony and cross-frequency coupling predict human memory formation. *ELife*, *3*, e05352. https://doi.org/10.7554/ELIFE.05352

Szalárdy, O., Simor, P., Ujma, P., Jordán, Z., Halász, L., Erőss, L., Fabó, D., & Bódizs, R. (2021). Sleep spindles, ripples, and interictal epileptiform discharges in the human anterior and mediodorsal thalamus. *BioRxiv*, 2021.08.12.456047. https://doi.org/10.1101/2021.08.12.456047

Weber, F. D., Supp, G. G., Klinzing, J. G., Mölle, M., Engel, A. K., & Born, J. (2020). Coupling of gamma band activity to sleep spindle oscillations – a combined EEG/MEG study. *NeuroImage*, 117452. https://doi.org/10.1016/J.NEUROIMAGE.2020.117452

Zhang, D., Snyder, A. Z., Shimony, J. S., Fox, M. D., & Raichle, M. E. (2010). Noninvasive Functional and Structural Connectivity Mapping of the Human Thalamocortical System. *Cerebral Cortex*, *20*(5), 1187–1194. https://doi.org/10.1093/cercor/bhp182

Zhang, H., Fell, J., & Axmacher, N. (2018). Electrophysiological mechanisms of human memory consolidation. *Nature Communications*, *9*(1), 4103. https://doi.org/10.1038/s41467-018-06553-y

Supplementary material

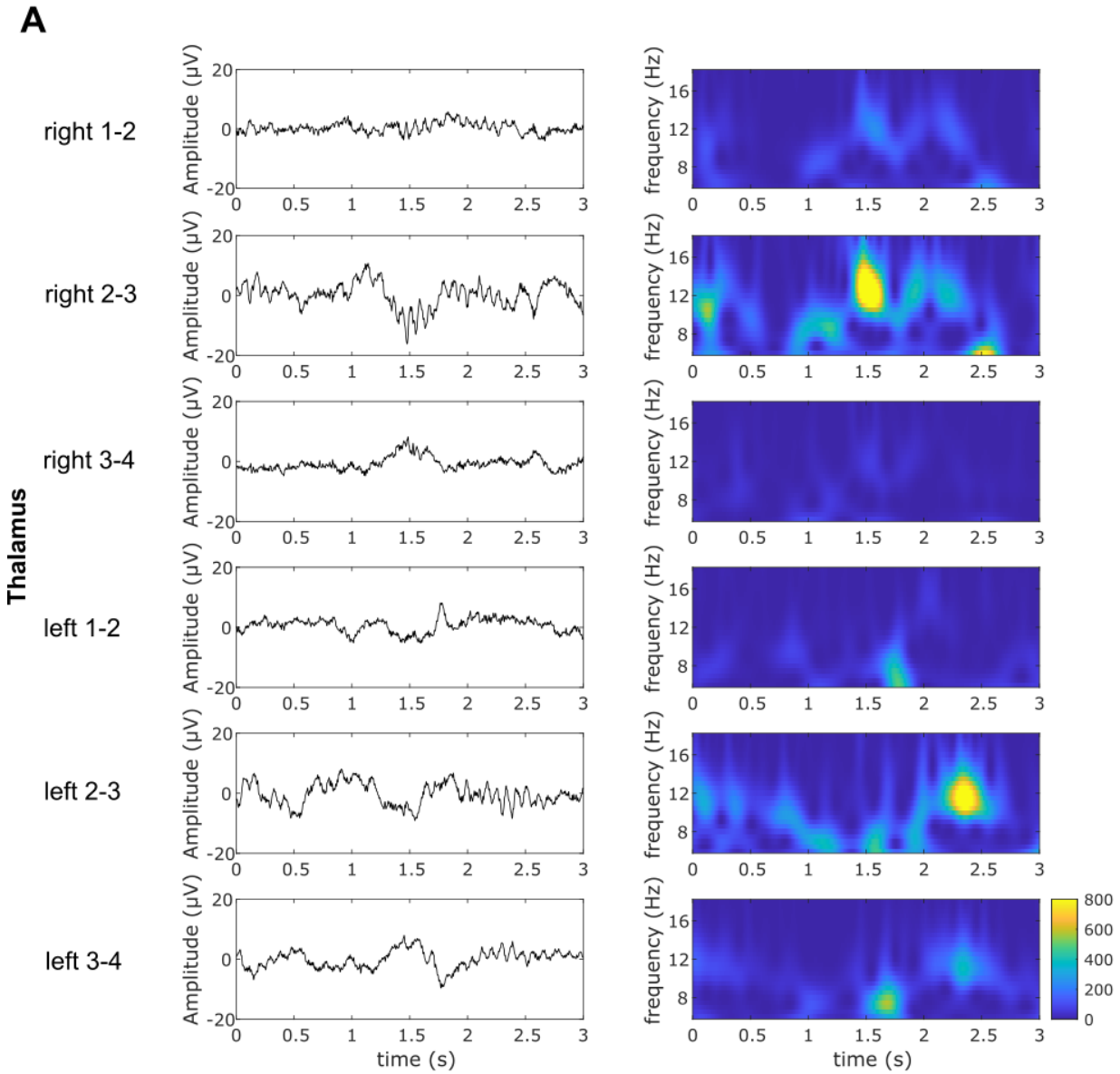

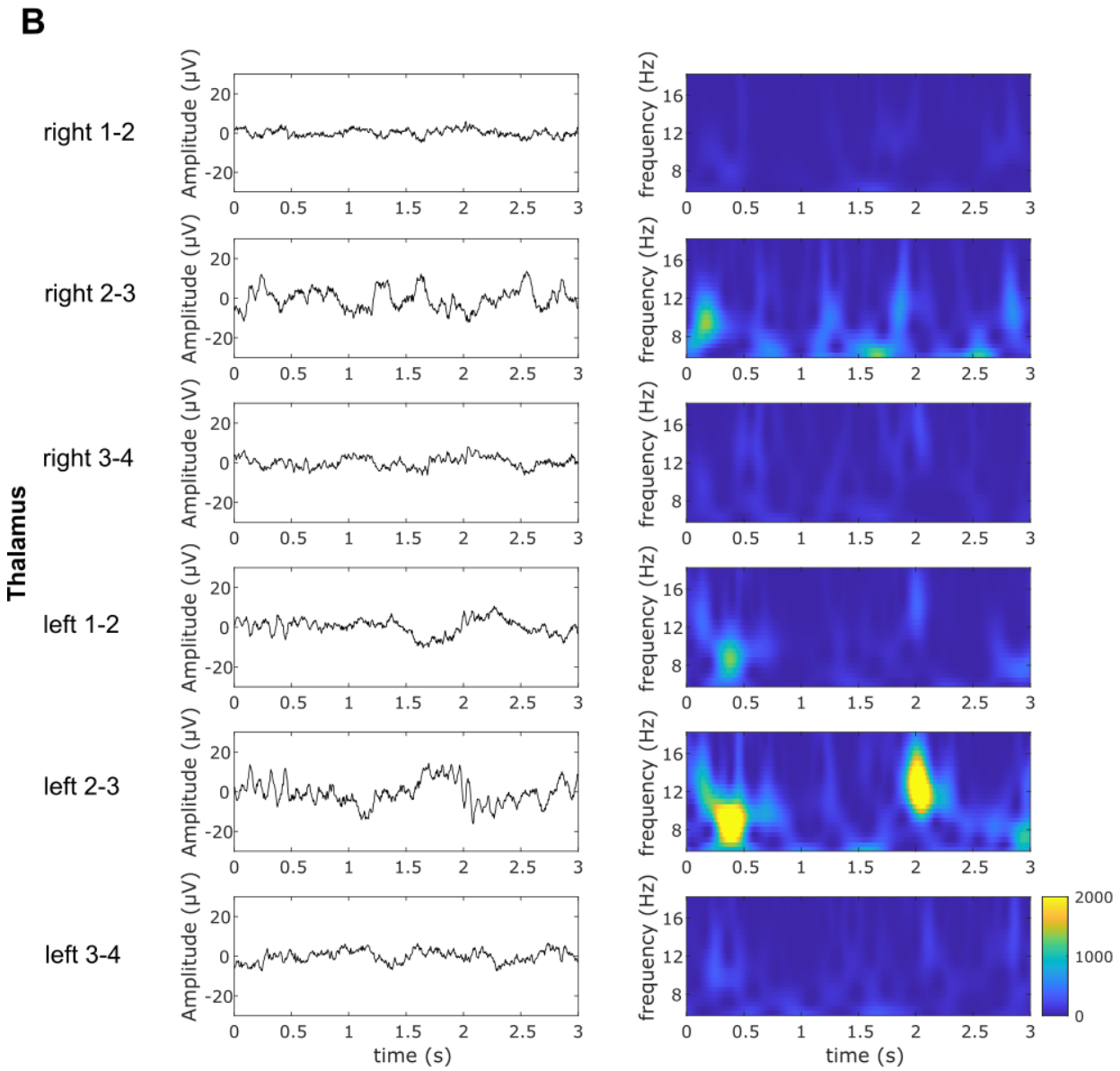
B
Thalamus
right 1-2
right 2-3
right 3-4
left 1-2
left 2-3
left 3-4
Amplitude (μV)
frequency (Hz)
time (s)
2000
1000
0

1056

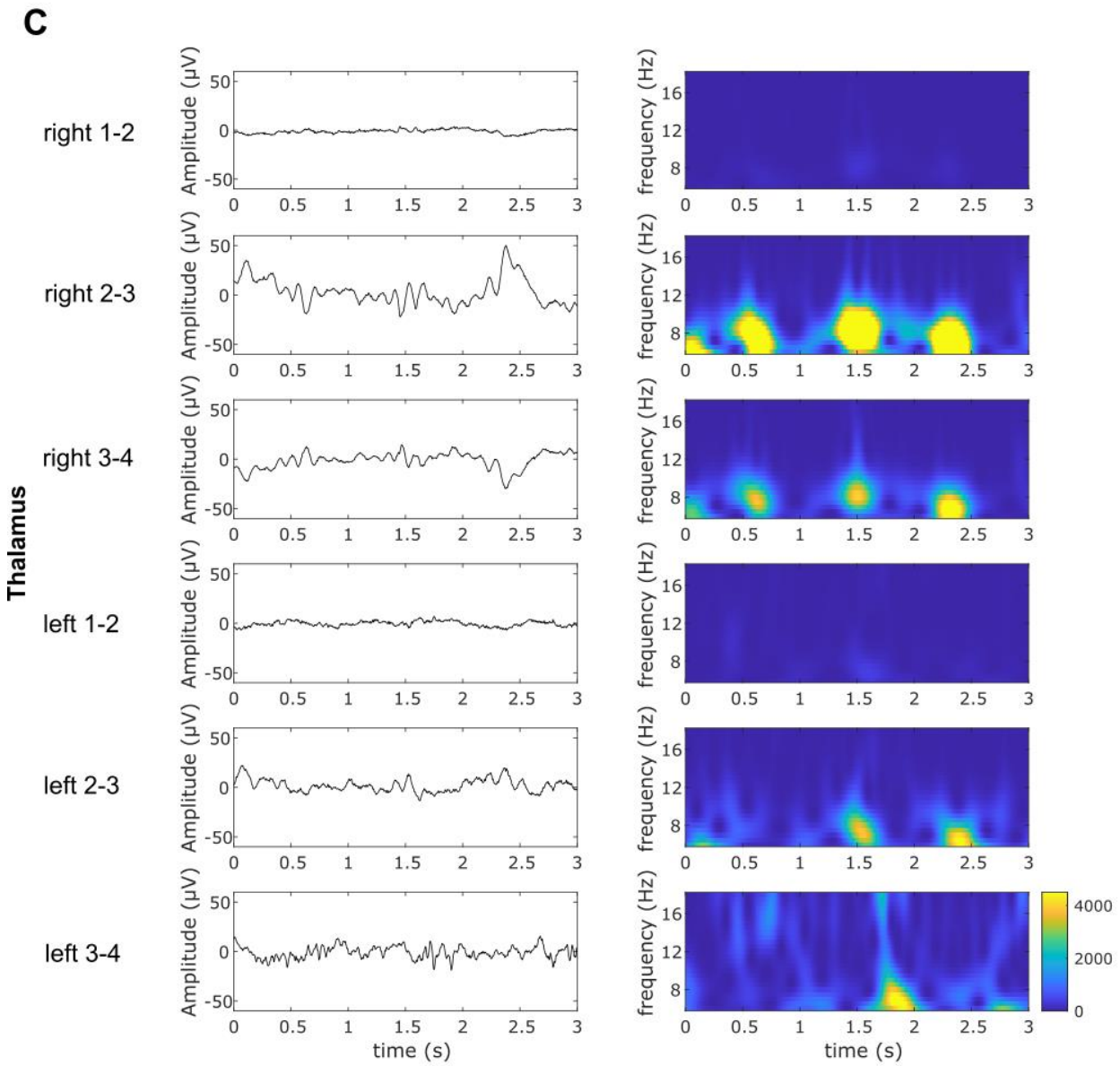

Supplementary figure 1. Representative data of thalamic spindles, shown in raw trace (left column) and time-frequency representations (TFRs; right column) from three different participants. **A)** A fast spindle in right thalamus (channel 2-3) at 1.5s is accompanied by a slow spindle in left thalamus (channel 3-4). This spindle is, in consequence, bilateral. At 2.3s, a unilateral spindle in the left thalamus occurs (channels 2-3 and 3-4). **B)** A slow bilateral spindle (channels right 2-3, left 1-2 and left 2-3) occurs at the beginning of the epoch. Though the peak of these spindles occurs at different time points, the tails of the spindles overlap, qualifying them as co-occurring spindles in our analysis. At 2s, we see a local fast spindle in channel left 2-3. **C)** A unilateral spindle

in the right thalamus (channels 2-3, 3-4) at 0.5s, followed by bilateral spindles at 1.5s and 2.3s in the right (channels 2-3 and 3-4) and left (left 2-3, and partially left 3-4) thalamus.

P	ANT	VA	RT	Lam.med.	MD
1		7.51, -6.25, 7.88 9.02, -4.90, 9.03 -7.92, -6.28, 8.96 -9.51, -5.73, 10.40	6.00, -7.61, 6.73 -6.34, -6.83, 7.52	4.49, -8.96, 5.58 -4.75, -7.38, 6.08	
2		7.40, -8.25, 10.65 -6.88, -8.53, 7.51 -8.82, -8.13, 8.77 -10.75, -7.72, 10.02		4.24, -9.40, 7.11 5.82, -8.82, 8.88 -4.95, -8.94, 6.26	2.65, -9.97, 5.33
3		6.95, -7.92, 8.96 8.72, -7.43, 10.52 - 7.77, -7.02, 8.45 -9.28, -6.85, 10.22	[1] -4.74, -7.37, 4.90 -6.25, -7.20, 6.67	5.19, -8.41, 7.39 [1]	3.42, -8.90, 5.82
4	4.35, -5.01, 11.70 5.87, -3.67, 12.03 -5.51, -6.84, 9.23 -6.73, -5.44, 9.98	[2]	7.39, -2.33, 12.36 8.90, -0.98, 12.68 -7.95, -4.03, 10.73[2] -9.17, -2.63, 11.48		
5		7.15, -7.65, 9.18 9.08, -7.80, 9.99 11.00, -7.96, 10.79 -8.50, -7.46, 8.69 -8.50, -7.46, 8.69 -11.76, -5.60, 10.14	5.23, -7.50, 8.37 -6.87, -8.39, 7.97		
6	4.50, -5.26, 8.32 5.97, -4.22, 9.70	-7.33, -5.52, 8.35 -8.86, -4.53, 9.48 [3]	7.44, -3.18, 11.08[3] -5.80, -6.52, 7.23		3.04, -6.29, 6,95 -4.27, -7.51, 6.11

7	7.29, -8.30, 7.73	4	5.80, -9.08, 6.37[4]
	8.78, -7.53, 9.10	5	-6.47, -8.40, 7.34[5]
	10.27, -6.75, 10.46		
	-8.43, -7.82, 8.13		
	-10.39, -7.25, 8.92		
	-12.35, -6.67, 9.71		

Supplementary Table 1. Coordinates in MNI-space (with respective nuclei guided by the Mai atlas) of the locations of electrode centers for all participants. Abbreviations: ANT: anterior nucleus of the thalamus; VA: ventral anterior nucleus; RT: Reticular nucleus; Lam.Med.: Lamina medialis; MD: mediodorsal nucleus
Electrode locations at borders between nuclei are indicated by superscripts.

Spindle characteristics per nucleus

We evaluated descriptive spindle measures when categorizing the data into their corresponding thalamic nuclei, selecting the three most common nuclei in our data. Note, that there was considerable uncertainty associated with the anatomical labeling. Three separate generalized linear mixed-effects models were constructed with density, duration, or amplitude as dependent variable, spindle type (slow vs. fast), thalamic nucleus (VA, ANT, RT) and their interaction as fixed effects, and participant as random intercept. The two-tailed significance level was set at $\alpha = 0.05$. Mixed-effects models were computed using the Matlab function *fitglme*.

In the generalized linear model (GLM) analysis, there was a significant main effect of spindle type ($F_{1,60} = 60.45$; $p < 0.001$) on spindle density, but no main effect of nucleus ($F_{2,60} = 1.48$; $p = 0.24$) and no significant interaction of spindle type and nucleus ($F_{2,60} = 2.29$; $p = 0.11$) on spindle density. Post-hoc comparisons revealed that slow spindles (6.90 ± 2.88 sp/min) had significantly higher density ($t(60) = 7.78$; $p < 0.001$) than fast spindles (2.94 ± 1.52 sp/min). The intercept term was significant ($F_{1,60} = 243.01$; $p < 0.001$), pointing to inter-individual differences in spindle density.

When modelling spindle duration with nucleus, spindle type and their interaction as mixed effects, and participant as random intercept, there was no significant effect of spindle type ($F_{1,60} = 4.01$, $p = 0.05$), nucleus ($F_{2,60} = 0.49$, $p = 0.62$), or their interaction ($F_{2,60} = 0.35$; $p = 0.71$), but a significant intercept ($F_{1,60} = 1033.5$, $p < 0.001$). When modeling spindle amplitude, there was a significant main effect of spindle type ($F_{1,60} = 6.80$; $p = 0.01$), but no significant main effect of nucleus ($F_{2,60} =$

0.40, p = 0.67) and no interaction effect of spindle type and nucleus ($F_{2,60}$ = 1.63; p = 0.20). Post-hoc comparisons revealed that slow spindles (9.96 ± 5.53 µV) had significantly higher amplitude (t(60) = 2.61; p = 0.01) than fast spindles (7.67 ± 5.85 µV) The intercept was significant ($F_{1,60}$ = 36.47, p < 0.001), suggesting inter-individual differences in both spindle duration and amplitude.

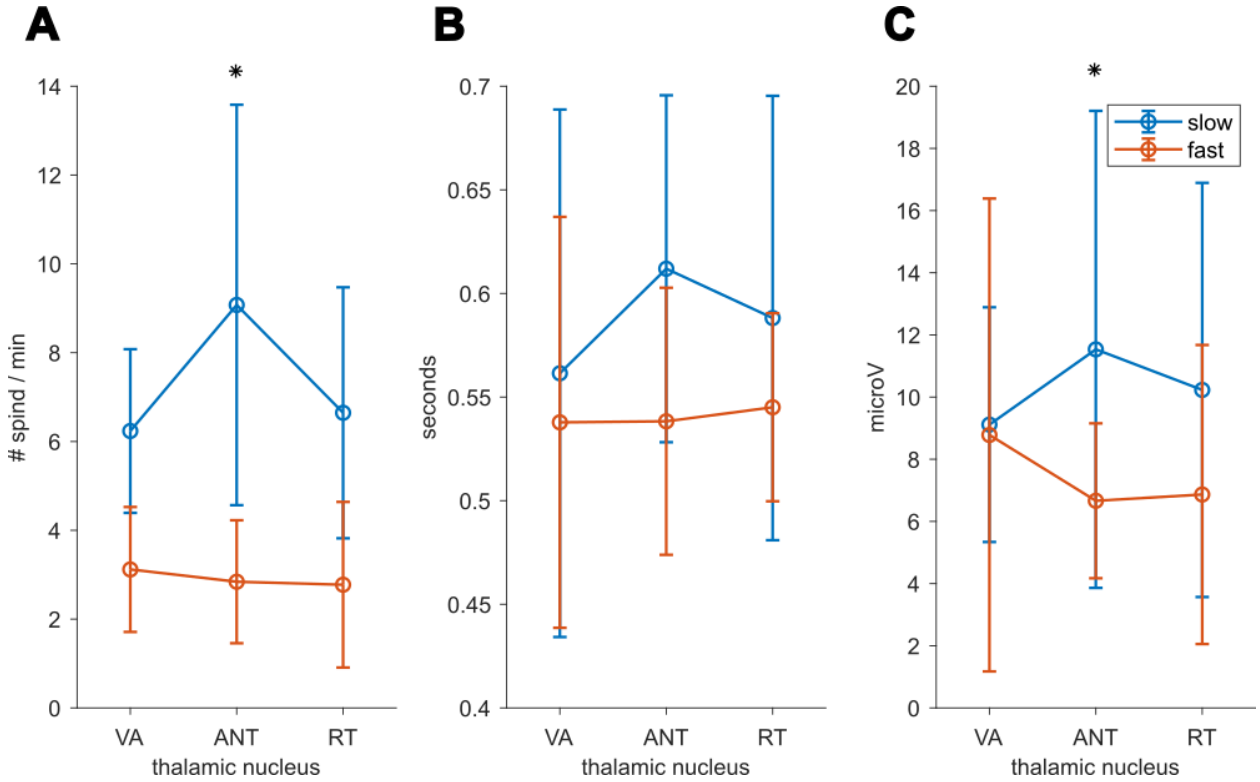

Supplementary figure 2. Average spindle characteristics per putative thalamic nucleus (see methods for limitations when estimating thalamic electrode locations). Values are shown for **A)** density; **B)** duration and **C)** amplitude. Asterisks mark significant results of spindle type at p < 0.05 in generalized linear mixed model. VA: ventral anterior nucleus of the thalamus; ANT: anterior nucleus of the thalamus; RT: Reticular nucleus of the thalamus.

Simultaneous spindle onset in anterior thalamus and cortex

The previous analyses have shown that spindles tend to co-occur systematically. In order to understand this co-occurrence better, we investigated potential shifts in onset of thalamic and cortical spindles. Thalamic spindles might precede or follow cortical spindle activity. On the one hand, this would allow inferences on a causal relation of spindles between the two regions, but on the other hand this temporal shift would bias analyses of spatiotemporal spindle overlap toward channel pairs with a smaller temporal offset. The temporal shift was investigated by means of lag

analysis. The lag was calculated as the time difference between spindle onsets in cortical relative to thalamic channels. Consequently, spindles with an earlier onset in the thalamus are indicated by a positive lag, and spindles with an earlier onset in cortical channels by a negative lag. Supplementary figure 3 depicts the median thalamocortical lag across participants and channels, for slow (A) and fast spindles (B), respectively. The distributions of thalamocortical lag for both slow (0.001 s ± 0.043) and fast (0.004 s ± 0.075) spindles were centered around 0. A one-sample t-test showed that both the slow ($t(778) = 0.35$; $p = 0.72$) and the fast ($t(797) = 1.45$; $p = 0.15$) spindles did not differ significantly from 0. This implies that spindle onset in thalamus and cortex was, on average, simultaneous.

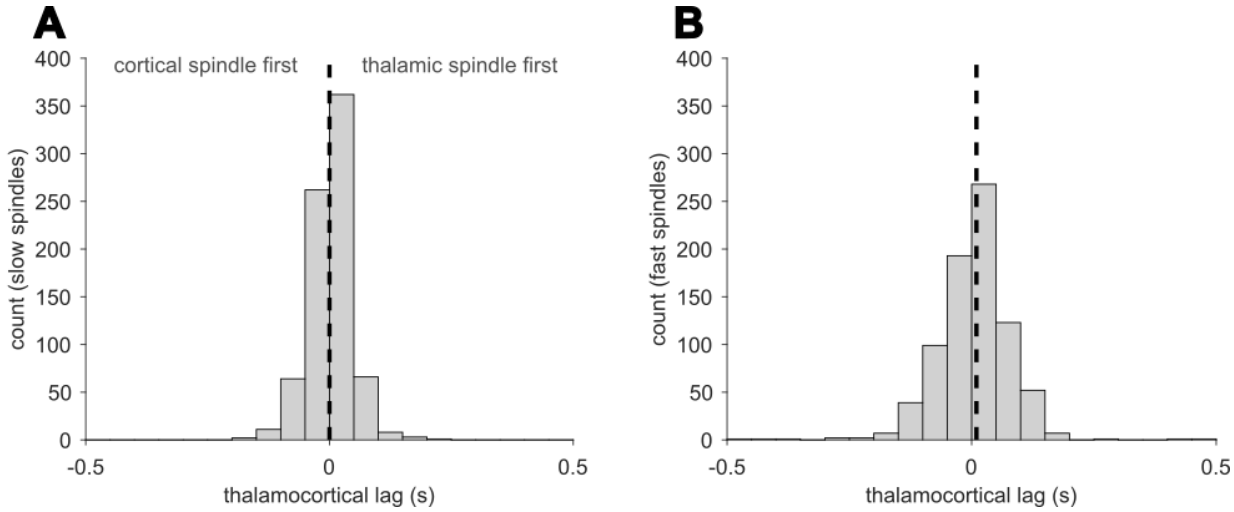

Supplementary figure 3. Histograms of thalamocortical lag of spindle onset across all thalamocortical channel pairs and participants. A positive lag indicates spindle onset in thalamus first, a negative lag in cortex first. **A)** slow spindles; **B)** fast spindles. Dashed line marks the median lag of cortical relative to thalamic spindle onset.